Volume 2 Issue 2
DECEMBER 2022
e-ISSN: 2822-6976

ADVANCED UAV

ADVANCED UAV

About the Journal

The Journal of ***Advanced UAV*** is a peer-reviewed journal that publishes studies on UAV development, use, and earth sciences and is scanned in International Indexes and Databases. The journal Advanced UAV (AUAV), Unmanned Aerial Vehicle Systems (UAS), and Remote Piloted Aircraft Systems (RPAS), etc. focuses on the design and applications of unmanned aerial vehicles, including. Likewise, contributions based on unmanned water/underwater drones and unmanned ground vehicles are also welcomed.

Aim & Scope

- UAV History, Legal and Legal Status in the World and Turkey
- UAV Production and Exportation
- UAV use in military areas (Air-Navy-Army Forces)
- Use of UAVs in Conventional (Traditional) and Modern Wars
- UAV Threats and Security Management
- UAV Sensors
- Augmented Reality and Virtual Reality Applications with UAV
- Basic UAV Applications,
- Fire Monitoring with UAV
- Documentation Studies with UAV
- UAV Photogrammetry and Remote Sensing with UAV,
- UAV LiDAR and Applications,
- Forestry Applications with UAV,
- Highway Projects with UAV,
- Geographical Information Systems Applications with UAV,
- Industrial Measurements with UAV,
- Deformation and Landslide Measurements with UAV,
- Mining Measurements with UAV,
- Urban Planning and Transportation Planning Studies with UAV,
- Precision Agriculture Practices with UAV,

CONTENTS

Volume 2 Issue 2

RESEARCH ARTICLES

Advanced UAV

http://publish.mersin.edu.tr/index.php/uav

e-ISSN 2822-6976

Study on the use of unmanned aerial vehicles in open mine sites: A case study of Ordu Province Mine Site

Alperen Erdoğan [*1], Mahmut Görken [1], Adem Kabadayı [1]

[1]*Yozgat Bozok University, Sefaatli Vocational School, Türkiye,* alperen.erdogan@bozok.edu.tr; mahmut.gorken@bozok.edu.tr; ademkabadayi@bozok.edu.tr

Cite this study: Erdoğan, A., Görken, M., & Kabadayı, A. (2022). Study on the use of unmanned aerial vehicles in open mine sites: A case study of Ordu Province Mine Site. Advanced UAV, 2 (2), 35-40

Keywords
UAV
Open Mines
UAV advantages
Photogrammetry

Research Article
Received: 01.10.2022
Revised: 04.11.2022
Accepted: 15.11.2022
Published: 30.11.2022

Abstract

Today, UAVs, which help to produce data with remote sensing and photogrammetry techniques, were used for military purposes at first. Unmanned aerial vehicles (UAV), which is a new sensor platform with the developing technology, has found many uses due to its fast, precise and repetitive measurement capabilities. In open mining areas, which is one of these areas, the topographic measurement problem emerges as a problem that needs to be overcome. The fact that the mine fields cover large areas, the measurements take a long time and are costly have made the use of UAVs a necessity. Aerial monitoring of open mining sites, together with the use of UAVs, is used in planning and calculations as an aid in areas such as mine production planning, blasting yield fields, determination of equipment locations, ore production and land application, volumetric calculations, monitoring of slope sensitivities and changes, security. It enables some data to be obtained quickly, reliably and cost-effectively. In this study, the structure of UAVs, the advantages of their use in open mining areas, their areas of use and their benefits for studies are explained.

1. Introduction

The ever-advancing and boundless technology has allowed man-made aircraft and related industries to change rapidly. The aviation adventure, which started with the dream of seeing the world from a bird's eye view and continued for the purpose of passenger and goods transportation, gained a different meaning with the First World War. Because in this great war, airplanes entered military service for the first time and served for offensive, defensive and reconnaissance purposes throughout the war [1].

For the first time in history, an unmanned vehicle was used in a military incident recorded as the first unmanned aerial attack. This happened in 1849, when the Austrians sent unmanned balloons filled with explosives to Venice, Italy. For the first time, the development and production of airplanes for the purpose of flying remotely, that is, unmanned, coincides with the First World War. Unmanned Aerial Vehicles, briefly UAVs, which are defined as flying vehicles that do not contain humans and can be controlled from the ground thanks to a communication system, have been actively used especially after the Second World War [2].

Drones, which are frequently used for civilian purposes other than military purposes, and especially used by today's younger generation born in the 2000s, are preferred because they outperform humans in many areas. Civil aviation unmanned aerial vehicles provide great benefits in fields such as journalism, show business, marketing, agriculture, cargo, health, emergency aid, communication, cartography and fire response.

Developing technology and demands have accelerated the development of UAVs and many studies have been carried out to achieve different missions and purposes, especially in recent years. These aircraft, which were discovered to be used for military purposes rather than civil aviation, serve the defense industry due to the numerous advantages they provide today. In the field of military aviation, Unmanned Aerial Vehicles are used as target designation and bait, in reconnaissance and surveillance conflicts and in high-risk missions [3].

UAVs provide great advantages over normal aircraft due to their low production, purchasing, fuel and flight costs [4-5]. More importantly, these vehicles do not pose a risk of injury or loss of life during the mission, as they are uncrewed. For the same reason, they are lighter than conventional aircraft and can stay in the air longer with the same amount of fuel [6].

On the other hand, the disadvantages of UAVs are that their danger detection abilities are not as strong as a human, they can pose a danger in case of loss of ground control connection, and manned aircraft are vulnerable to air attacks. However, these disadvantages are tried to be minimized with research and development activities in data transfer and artificial intelligence technologies. On the other hand, further increasing flight times will allow these vehicles to be used widely in the near future [7].

Today, Turkey has managed to become a country that produces its own software and technology in the defense industry. In addition to the defense industry, UAVs are used in applications such as virtual reality and three-dimensional (3D) model production. In addition, UAVs provide effective and efficient use in the detections and post-disaster investigations, tourism, architectural areas and 3D city planning, and 3D modeling of structures before the disaster occurs [8].

Compared to images obtained from traditional aerial photogrammetry, high-precision images can be produced at low cost in low-altitude flights with the help of UAVs [9-10]. Unlike the vehicles used in traditional aerial photogrammetry, UAVs offer the opportunity to fly close to the object and at low altitudes. In some cases where transportation is difficult and manned aircraft cannot be used, UAVs are preferred as an alternative method. In addition, despite the unnecessary data volume and high cost in small-scale conventional aerial photogrammetry applications, a great deal of savings can be achieved by using UAVs. Studies carried out with the help of UAVs approach the sensitivity of terrestrial photogrammetry and find application opportunities in many different areas due to the fact that the data processing process can be completed in a short time [11]. Twenty years ago, robotic total station was used frequently [12]. However, in recent years, UAV technology has been widely used by many disciplines for different purposes (map production, volume calculations, 3D model making, documentation of cultural heritage and hobby purposes, etc.).

Uysal et al. [13] aimed to produce the Digital Terrain Model (DTM) of the Şahitler Kayası Mound using UAV photogrammetric techniques and to perform an accuracy analysis on an area of approximately 5 ha in the Şahitler Kayası location in the center of Afyonkarahisar. In their study, they established a total of 27 GCPs, 5 of which are homogeneous, and obtained the coordinates of the GCPs in the ITRF96 datum with the Stonex S9 GNSS (Global Navigation Satellite Systems - Global Positioning Satellite Systems) device using the RTK method. Images were taken with the Canon EOS digital camera on the UAV from an average height of 60 m. As a result of their studies, they evaluated the accuracy of DTM with 30 control points and determined a vertical accuracy of 6.62 cm. They stated that the combination of UAVs and photogrammetric techniques will provide significant contributions to the studies to be carried out in this field in terms of accuracy, speed, cost and product diversity. UAVs are one of the most important technologies in many aviation applications, especially for civil and military purposes, due to their low cost and high performance. Although UAVs have short wingspan (fixed or rotating wings) and a light structure, they have a sensitive structure during flight [14-15].

Şenol and Kaya [16] stated that field work of the model should be done to create a 3D model. In order to reveal the 3D model of a structure, they included UAV data collection in their data collection method. In particular, they wanted to minimize the field studies by using the data collection method with the UAV, and for this purpose, they were able to collect data without the need for fieldwork. They also reported that models can be created from images of UAV, terrestrial and rough areas with various software. Measurements made with classical terrestrial methods are difficult, expensive, take a lot of time compared to the photogrammetric method and are not possible due to the nature of some lands. It has become a necessity to prefer various alternative methods in mountainous, rocky and rough terrains where people have difficulty in transportation. With classical measurement methods, it may not be possible to approach dangerous places such as swamps, stream beds and sometimes the edge of a cliff. With UAVs, it is now possible to easily access areas that people cannot reach and have difficulty in taking images. With the overlay images to be taken from the land, the terrain structure can be modeled in 3D and coordinates [17].

Expanding the use of UAVs in mapping rough areas will provide many advantages. Especially in very hilly areas, mapping processes should be done in a short time, and mapping work should be done in stock movements and incubation calculations in the field. Conducting this study with terrestrial methods may create risks in terms of occupational safety, increase costs and cause loss of time. In addition, it provides significant advantages in terms of cost, time and personnel in the production of periodic orthophoto maps using UAVs. In addition, periodic maps of the entire field can be produced with the UAV instead of mapping only within the area where the study is carried

out or within a certain region. Thus, it will be possible to make optimum planning by ensuring that potential threats can be predicted in the work area and healthy decisions will be made for the future [18].

Today, UAV is frequently used in cultural heritage studies [19-21]. Photogrammetry and UAVs have been used in land cover classification [22], landslide modeling [23-24], rockfall modeling [25], pond area volume [26]. It has been used in many engineering projects such as measuring the location of inaccessible geological features [27], coastline detection [28], volume calculation [29].

2. Material and Method

The framework for acquiring and processing UAV images in open pit mining areas consists of four main parts. These are configuring the ground network and flight path design, obtaining images, mapping photos using GCPs with the help of photogrammetric software, creating DEM & ortho-images and drawing. First, the distribution of the ground control network was measured by the Turkish National Basic GNSS Network-Active (TUSAGA-Active) System. The flight path has been designed considering specific factors for UAV-based photogrammetric and aerial image guidance. During autonomous flight operations, both UAV images and position and guidance system data are obtained. Orthophoto and DEM maps are created in Pix4D software, which is used as photogrammetric software.

The technical specifications of the FC6310R camera system attached to the Phantom 4 Pro RTK UAV used in the study are shown in Table 1.

Table 1. FC6310R Technical Specifications

Property	Orthophoto	Digital Elevation Model
Row and Column	2886 *2886	2886*2886
Band no	3 (RGB)	1
Pixel type	Unsigned integer	Unsigned integer
Radiometric resolution	8 bit	32 bit
Coordinate system	TUREF/TM39	TUREF/TM39
Zone	37	37

The images were obtained on the open mine site in Ünye district of Ordu province (Figure 1). The mine site was excavated during the bed determination studies and as a result of the estimations, its operations were stopped. The biggest support to these studies has been the UAVs, which enable them to have fast measurement and information about the area. The study area is 13 ha, and 5 control points have been marked in addition to 9 ground control points (YKN) points, with reference to [30].

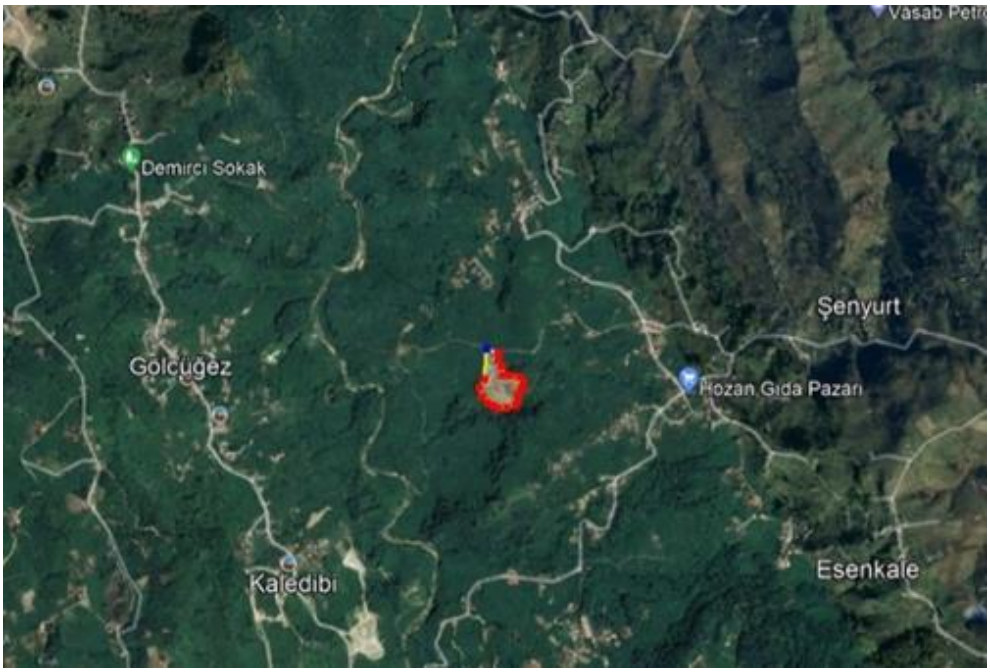

Figure 1. Study area

Coordinates of GCPs and control points (CP), were obtained with the GNSS receiver. GCPs and CPs were added to the Pix4D software according to their types, and the accuracy calculations given in the final report are shown in Table 2.

Table 2. Amount of error for CP

CP Number	X (cm)	Y (cm)	Z (cm)
1	4.1	3.9	3.5
2	3.8	3.1	3.2
3	2.5	2.7	2.4
4	1.9	3.1	5.1
5	3.7	2.2	3.6

Since the mine site is within the densely covered area, a problem occurred in the overlapping of the images outside the site (Figure 2).

Figure 2. Densely covered area

An error occurred in the overlapping of the area marked with red in Figure 2 due to the dense pine cover, and in the second evaluation, the common points were manually marked and the error was eliminated. As a result of the evaluation, dense point cloud and orthophoto image were obtained. Digitization studies were carried out on the point cloud and transferred to the CAD program. As a result, an image of the land was made with the image dressed terrain model (Figure 3).

Figure 3. Pix4d Mesh İmage

The images were obtained on the open mine site in Ünye district of Ordu province (Figure 1). The mine site was excavated during the bed determination studies and as a result of the estimations, its operations were stopped. The biggest support to these studies has been the UAVs, which enable them to have fast measurement and information about the area. The study area is 13 ha, and 5 control points have been marked in addition to 9 ground control points (YKN) points, with reference to [30].

3. Conclusion

In the study, which was prepared with the aim of including unmanned aerial vehicles (UAV) in mining applications and revealing their usage potential, it is aimed to make more accurate and more practical measurements and calculations in shorter times in the mining sector of our country, which is working intensively in open pit mining.

In the study, with the use of unmanned aerial vehicles and appropriate software, the concepts such as volume and mass were studied on-site in areas that are difficult to calculate. It has been proven that studies can be carried out to determine the amount of extraction, which is one of the most important factors in mining operations. Considering the number of errors given in Table 1, it is seen that the UAVs are quite successful. UAV minimizes accidents that may occur during land measurements by highlighting occupational health and safety, especially in mining areas.

136 pictures were taken at the mine site, and 9 GCPs and 5 CPs were marked. While the work in the field took 1 hour and 15 minutes, the processing of the images and the production of the report took 29 minutes. The DSM and orthomosaic images produced are 3.1 cm resolution. By looking at these data, UAVs have proven their usability in open mining operations.

Funding

This research received no external funding.

Author contributions

Alperen Erdogan: Visualization, Writing-Reviewing and Editing, Conceptualization, Methodology, Software. **Mahmut Gorken:** Data curation, Writing-Original draft preparation, Software, Validation. **Adem Kabadayı:** Visualization, Investigation, Software, Validation

Conflicts of interest

The authors declare no conflicts of interest.

References

1. Kabadayi, A., Kaya, Y., & Yiğit, A. Y. (2020). Comparison of documentation cultural artifacts using the 3D model in different software. *Mersin Photogrammetry Journal*, *2*(2), 51-58.
2. Ulvi, A., Yakar, M., Yiğit, A. Y., & Kaya, Y. (2020). İHA ve yersel fotogrametrik teknikler kullanarak Aksaray Kızıl Kilise'nin 3 Boyutlu nokta bulutu ve modelinin üretilmesi. *Geomatik Dergisi*, *5*(1), 22-30.
3. Kabadayi, A. (2022). Maden Sahasının İnsansız Hava Aracı Yardımıyla Fotogrametrik Yöntemle Haritalanması. *Türkiye İnsansız Hava Araçları Dergisi*, *4*(1), 19-23.
4. Kaya, Y., Yiğit, A. Y., Ulvi, A., & Yakar, M. (2021). Arkeolojik alanların dokümantasyonununda fotogrametrik tekniklerinin doğruluklarının karşılaştırmalı analizi: Konya Yunuslar Örneği. *Harita Dergisi*, *165*, 57-72.
5. Ceylan, M. C., & Uysal, M. (2021). İnsansız hava aracı ile elde edilen veriler yardımıyla ağaç çıkarımı. *Türkiye Fotogrametri Dergisi*, *3*(1), 15-21.
6. Karabacak, A. (2021). İnsansız hava araçları (İHA) İle enerji nakil hatlarının ölçülmesi üzerine derleme. *Türkiye Fotogrametri Dergisi*, *3*(1), 1-8.
7. Ulvi, A., Yakar, M., Yiğit, A., & Kaya, Y. (2019). The use of photogrammetric techniques in documenting cultural heritage: The Example of Aksaray Selime Sultan Tomb. *Universal Journal Of Engineering Science*, *7*(3), 64-73.
8. Bryson, M., & Sukkarieh, S. (2004, December). Vehicle model aided inertial navigation for a UAV using low-cost sensors. In *Proceedings of the Australasian Conference on Robotics and Automation* (pp. 1-9). Australian Robotics and Automation Association.

9. Espositoa, S., Fallavollitaa, P., Wahbehb, W., Nardinocchic, C., & Balsia, M. (2014, July). Performance evaluation of UAV photogrammetric 3D reconstruction. In *2014 IEEE Geoscience and Remote Sensing Symposium* (pp. 4788-4791). IEEE.
10. Alptekin, A., Çelik, M. Ö., Kuşak, L., Ünel, F. B., & Yakar, M. (2019). Anafi Parrot'un heyelan bölgesi haritalandirilmasinda kullanimi. *Türkiye İnsansız Hava Araçları Dergisi*, *1*(1), 33-37.
11. Doğan, Y., & Yakar, M. (2018). GIS and three-dimensional modeling for cultural heritages. *International Journal of Engineering and Geosciences*, *3*(2), 50-55.
12. Yakar, M. (2009). Digital elevation model generation by robotic total station instrument. *Experimental Techniques*, *33*(2), 52-59.
13. Uysal, M., Toprak, A. S., & Polat, N. (2015). DEM generation with UAV Photogrammetry and accuracy analysis in Sahitler hill. *Measurement*, *73*, 539-543.
14. Jung, S. (2004). *Design and development of a micro air vehicle (MAV): test-bed for vision-based control* (Doctoral dissertation, University of Florida).
15. Yakar, M., & Yılmaz, H. M. (2008). Kültürel miraslardan tarihi Horozluhan'in fotogrametrik rölöve çalişmasi ve 3 boyutlu modellenmesi. *Selçuk Üniversitesi Mühendislik, Bilim ve Teknoloji Dergisi*, *23*(2), 25-33.
16. Şenol, H. İ., & Kaya, Ş. (2019). İnternet tabanlı veri kullanımıyla yerleşim alanlarının modellenmesi: Çiftlikköy Kampüsü Örneği. *Türkiye Fotogrametri Dergisi*, *1*(1), 11-16.
17. Yakar, M., & Doğan, Y. (2017). Uzuncaburç Antik Kentinin İHA Kullanılarak Eğik Fotogrametri Yöntemiyle Üç Boyutlu Modellenmesi. 16. *Türkiye Harita Bilimsel ve Teknik Kurultayı. TMMOB Harita ve Kadastro Mühendisleri Odası, Ankara*.
18. Unal, M., Yakar, M., & Yildiz, F. (2004, July). Discontinuity surface roughness measurement techniques and the evaluation of digital photogrammetric method. In *Proceedings of the 20th international congress for photogrammetry and remote sensing, ISPRS* (Vol. 1103, p. 1108).
19. Çelik, M. Ö., Yakar, İ., Hamal, S., Oğuz, G. M., & Kanun, E. (2020). Sfm tekniği ile oluşturulan 3B modellerin kültürel mirasın belgelenmesi çalışmalarında kullanılması: Gözne Kalesi örneği. *Türkiye İnsansız Hava Araçları Dergisi*, *2*(1), 22-27.
20. Korumaz, A. G., Dülgerler, O. N., & Yakar, M. (2011). Kültürel mirasin belgelenmesinde dijital yaklaşimlar. *Selçuk Üniversitesi Mühendislik, Bilim ve Teknoloji Dergisi*, *26*(3), 67-83.
21. Yakar, M., Kabadayı, A., Yiğit, A. Y., Çıkıkcı, K., Kaya, Y., & Catin, S. S. (2016). Emir Saltuk Kümbeti fotogrametrik rölöve çalişmasi ve 3boyutlu modellenmesi. *Geomatik*, *1*(1), 14-18.
22. Öztürk, M. Y., & Çölkesen, İ. (2021). The impacts of vegetation indices from UAV-based RGB imagery on land cover classification using ensemble learning. *Mersin Photogrammetry Journal*, *3*(2), 41-47.
23. Alptekin, A., & Yakar, M. (2020). Heyelan bölgesinin İHA kullanarak modellenmesi. *Türkiye İnsansız Hava Araçları Dergisi*, *2*(1), 17-21.
24. Kusak, L., Unel, F. B., Alptekin, A., Celik, M. O., & Yakar, M. (2021). Apriori association rule and K-means clustering algorithms for interpretation of pre-event landslide areas and landslide inventory mapping. *Open Geosciences*, *13*(1), 1226-1244.
25. Alptekin, A., Çelik, M. Ö., Doğan, Y., & Yakar, M. (2019). Mapping of a rockfall site with an unmanned aerial vehicle. *Mersin Photogrammetry Journal*, *1*(1), 12-16.
26. Alptekin, A., & Yakar, M. (2020). Determination of pond volume with using an unmanned aerial vehicle. *Mersin Photogrammetry Journal*, *2*(2), 59-63.
27. Yakar, M. (2011). Using close range photogrammetry to measure the position of inaccessible geological features. *Experimental Techniques*, *35*(1), 54-59.
28. Ünel, F. B., Kuşak, L., Çelik, M., Alptekin, A., & Yakar, M. (2020). Kıyı çizgisinin belirlenerek mülkiyet durumunun incelenmesi. *Türkiye Arazi Yönetimi Dergisi*, *2*(1), 33-40.
29. Kaya, Y., Şenol, H. İ., Memduhoğlu, A., Akça, Ş., Ulukavak, M., & Polat, N. (2019). Hacim Hesaplarında İHA Kullanımı: Osmanbey Kampüsü Örneği. *Türkiye Fotogrametri Dergisi*, *1*(1), 7-10.
30. Erdoğan, A., & Mutluoglu, O. (2020). İnsansız Hava Araçları ile Harita Üretim Çalışmalarında Farklı Yükseklikllerde Yapılan Uçuşların Konum Doğruluğuna Etkisi. *Türkiye İnsansız Hava Araçları Dergisi*, *2*(1), 28-35.

Advanced UAV
http://publish.mersin.edu.tr/index.php/uav
e-ISSN 2822-6976

The use of UAV photogrammetry in modeling ancient structures: A case study of "Kanytellis"

Engin Kanun*[1], Aydın Alptekin [2], Lale Karataş [3], Murat Yakar [4]

[1]Mersin University, Department of Mechanical Engineering, Türkiye, ekanun@mersin.edu.tr
[2]Mersin University, Department of Geological Engineering, Türkiye, aydinalptekin@mersin.edu.tr
[3]Mardin Artuklu University, Department of Architecture and Urban Planning, Türkiye, lalekaratas@artuklu.edu.tr
[4]Mersin University, Department of Geomatics Engineering, Türkiye, myakar@mersin.edu.tr

Cite this study: Kanun, E., Alptekin, A., Karataş, L., & Yakar, M. (2022). The use of UAV photogrammetry in modeling ancient structures: A case study of "Kanytellis". Advanced UAV, 2 (2), 41-50.

Keywords
Photogrammetry
UAV
3D Modeling
Digital Archiving
Cultural Heritage

Research Article
Received: 03.10.2022
Revised: 06.11.2022
Accepted: 16.11.2022
Published: 30.11.2022

Abstract

Investigations of the Antiquity and Late Antiquity have been carried out numerous times by historians and archaeologists, and these researches continue intensely. Archaeological discoveries and historical ruins provide information about the enigmatic history of humanity. Studies on ancient cities contribute to the social, cultural, administrative and economic analysis of the period. Within the scope of this study, an ancient village house in Kanytellis, an example of these ancient cities, was modeled in 3D and digitally documented. The area and volume calculations of the building are also presented in the study by taking measurements on the 3D model of the ancient village house. Analyzes were conducted by two different software (Agisoft Metashape and Context Capture) and the results were presented comparatively in the results section of the study. According to the analysis made between the models, a difference of 1.32 cm was calculated. It is thought that the model reconstructed will contribute to the aims of transferring Turkey's historical and cultural heritage to future generations and playing a role in developing tourism activities.

1. Introduction

Humanity has started to actively change the environment in which it lives and move to a settled life in order to meet its needs from the hunter-gatherer order that it has been living in for 2.5 million years [1]. Ancient and late antiquity are the ages when examples of settled life are seen [2-5]. It is of great importance to examine the historical remains and artifacts in order to learn the details of the social, cultural, economic, political, administrative, religious, etc. experiences of the societies in the historical process [6]. Ancient cities are among the regions where historical ruins and findings are densely encountered. The ancient city of Kanytellis in Mersin province of Turkey is one of these examples. Kanytellis, which includes structures such as houses, tombs and churches, is dated to the Late Antiquity. The buildings are placed in terraces in accordance with the structure of the topography. The areas between them form streets, some of which narrow down to 1-2 meters. The relatively wider openings between the buildings were used as small squares and cisterns were placed in most of them. A main street starting from the Hellenistic tower continues northward along the western border of the sinkhole. This city axis, which was formed in Antiquity, was preserved in Late Antiquity, although a part of it was closed by a church and narrowed in the northern part [2].

Modeling and digital archiving of historical buildings and artifacts serve the purpose of transferring cultural heritage to future generations [7-10]. Numerous methods are used in modeling processes and photogrammetry is one of these methods that is frequently utilized [8].

In this study, an ancient village house in Kanytellis was modeled by photogrammetric method using an unmanned aerial vehicle. As a result of the analyzes conducted on the model obtained, values such as lengths, areas and volume of the building are presented. Analyzes were conducted by two different software (Agisoft Metashape and Context Capture) and the results were presented comparatively in the results section of the study. Coordinate and length measurements were carried out on the models obtained with both software and the results were presented comparatively. As a continuation of this study, it is planned to analyze the thermal performance of the ancient house.

The location of the ancient house is shown in Figure 1.

Figure 1. The location of the ancient house

2. Material and Method

This study is composed of two phases, namely field and office work. The steps of controlling the study area, preparing it for photographing and taking images of the ancient house by an unmanned aerial vehicle constitute the field study phase. When it comes to the office work phase, the steps of transferring the data received from the unmanned aerial vehicle to the computer environment, interpreting and processing were performed.

UAV photogrammetry has been used frequently in engineering projects in the last decade. Objects can be modelled without touching them using UAV [11-13]. Rockfall [14], landslide studies [15-16], pond volume [17], shoreline detection [18], village site modelling [19], material deterioration [20].

2.1. Field work

The field studies first started with the necessary permissions from the relevant museum directorate. The antique village house, which is an ancient artifact built in the 2nd century AD and located in the Kanlıdivane region of the Mersin province of Türkiye, has coordinates 36.526774, 34.177668. The ancient house is located in the northwest of the sinkhole.

Then, the flight altitudes at which images will be taken around the house were determined. Images were taken by Parrot Anafi HDR drone (Figure 2) by manually. The technical specifications of the unmanned aerial vehicle utilized are presented in Table 1. Some of the images of the antique village house are shown in Figure 3.

Although there are automated flight plans, the flights were made manually in order to get all the desired details on the structure. Every detail of the structure was tried to be captured by flying first at low altitude and then at high altitude. A total of 107 images were taken. Some of the images of the ancient house captured are shown in Figure 3.

Figure 2. Parrot Anafi HDR UAV

Table 1. The technical specifications of the UAV

	Feature	Value
Drone	Size folded	244x67x65 mm
	Size unfolded	175x240x65 mm
	Weight	320 g
	Max transmission range	4km with controller
	Max flight time	25 min
	Max horizontal speed	15 m/s
	Max vertical speed	4 m/s
	Max wind resistance	50 km/h
	Service ceiling	4500m above sea level
	Operating temperature	-10°C to 40°C
Lens	Sensor	1/2.4'' CMOS
	Aperture	f/2.4
	Focal length (35 mm eq.)	23-69 mm (photo)
	Depth of field	1.5 m - ∞
	ISO range	100-3200
	Digital zoom	up to 3x (4K Cinema, 4K UHD, FHD)
	Photo resolution	21MP (5344x4016) / 4:3 / 84° HFOV

Figure 3. Some images of the antique village house captured by UAV

2.2. Camera Calibration

The camera utilized should be calibrated beforehand so that the merging and overlay operations of the images can be of high accuracy. The unmanned aerial vehicle used in this research has a 5.92 mm sensor, as was indicated in the part before it. Images have a size of 4608x3456 pixels. Camera calibration was conducted in Context Capture software. The distortion parameters obtained as a result of camera calibration is shown in Table 2.

Table 2. Camera calibration parameters

	Focal Length [mm]	Focal Length (eq. 35) [mm]	Principal Point X [px]	Principal Point Y [px]	K1	K2	K3	P1	P2
Previous Values	3.74	22.75	2301.24	1754.28	-0.0015	0.0087	-0.0058	0.0022	0
Optimized Values	3.83	23.31	2325.78	1729.62	-0.0041	0.0142	-0.0112	0.0036	0.0003
Difference Previous / Optimized	0.09	0.57	24.54	-24.66	-0.0026	0.0055	-0.0054	0.0014	0.0003

2.3. Office work

After the completion of the image acquisition within the scope of the field work, the office work phase was initiated. Firstly, the data received from the flight were transferred to the computer environment. The total size of the image file acquired followed the flight was 517 MB. Data processing was conducted in Bentley's Context Capture, and Agisoft Metashape software as well. The office work, which was started after half a day of field work, was completed in two days. The positions of the images taken relative to the ancient house are presented in Figure 4.

Figure 4. The positions of the images taken by UAV

All the photos captured were utilized in the processes. Generic block type was chosen for the aerotriangulation process of the images based on experience from previous studies. No control point was used in this study. Positioning metadata of the images were utilized for rigid registration. High key points density option was selected. In the aerotriangulation process, 97377 tie points were formed in Agisoft, while 31390 tie points had been occurring in Context Capture software. Alignment steps of the images took 4 min 25s for Agisoft and 6 min 41s for Context Capture.

Reconstruction process was initiated by generic selection of matching pairs after aerotriangulation step. Extra geometric precision (tolerance of 0.5 pixel in input photos) option was implemented. In order not to deviate from the original geometry of the house, small hole-filling option was applied. Finally, in this step, the spatial frame is reduced, avoiding the modeling of unnecessary regions and the use of excessive computer power. After the aerotriangulation process, it took 1 hour and 28 minutes to recreate the 3D solid model. Computer used in

processes has Intel(R) Core (TM) i7-7700HQ CPU @2.81GHz processor, 16 GB of RAM capacity and GeForce Nvidia 1050 Ti 4 GB graphics card.

The above operations were performed in Context Capture software and the same operations were repeated in Agisoft software. It took 1 hour and 13 minutes to obtain the 3D solid model of the ancient house.

Following the process of recreating 3D solid models, coordinate and length measurements were conducted on the model in both software. Obtained values are presented comparatively in the "Results" section.

3. Results

After the camera calibration, field and office work phases were complemented, a 3D solid model of the antique village house was obtained. The surface texture was produced by utilizing images to attach visuality to the obtained 3D solid model. Texture compression quality was selected as 100% quality and texture sharpening option was enabled. The three-dimensional models of ancient house are presented in Figure 5a and Figure 5b.

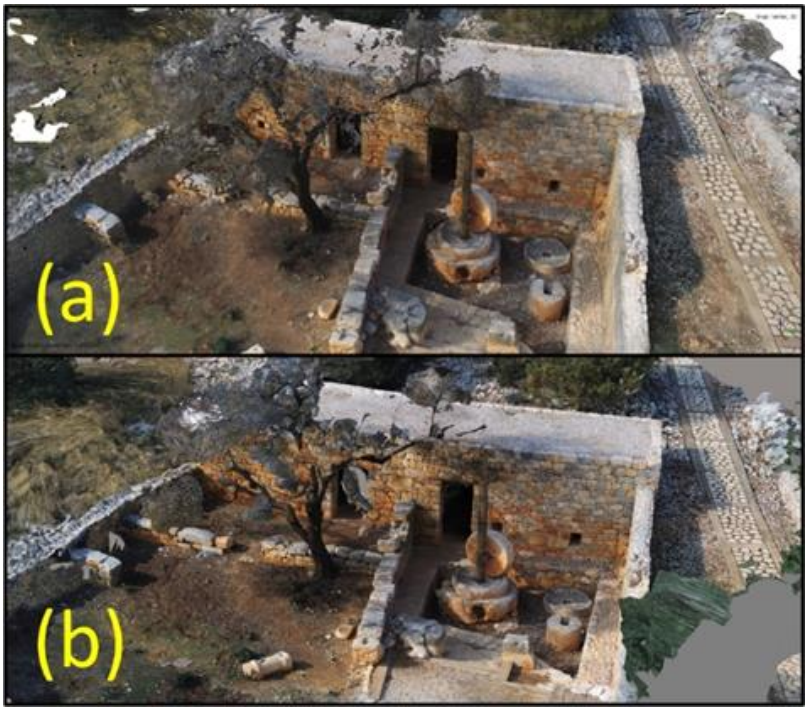

Figure 5. 3D models of the ancient house (a-Agisoft; b-Context Capture)

The final 3D models are in one-to-one scale with the real work. While length measurements can be taken on the model, area and volume calculations can be made at the same time. Examples of area and volume calculations on the building are presented in the Figures 6-7-8.

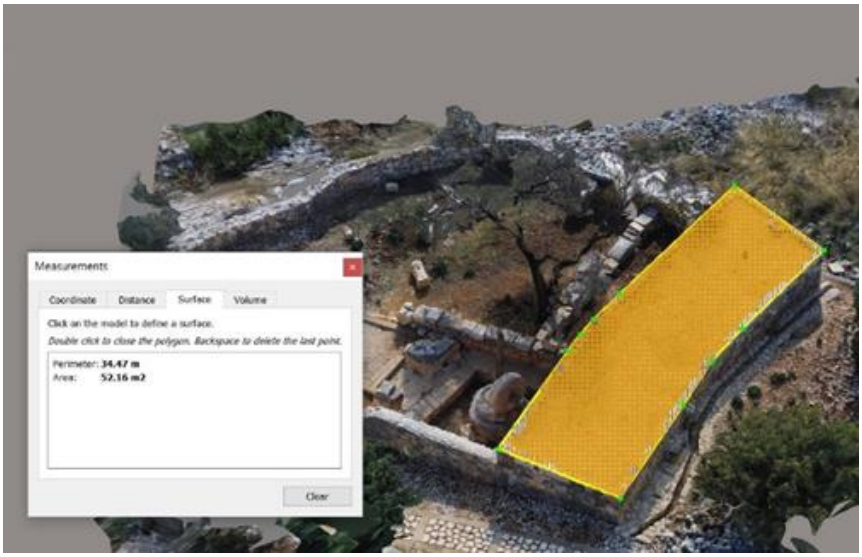

Figure 6. Floor area of the antique house

Figure 6 indicates the floor area of the ancient house, which is 52.16 m^2. In addition, the perimeter of the floor area was calculated as 34.47 m. The building height is 3.29 meters and as a result of multiplying this value by the floor area, the building volume is calculated as 171.6 cubic meters.

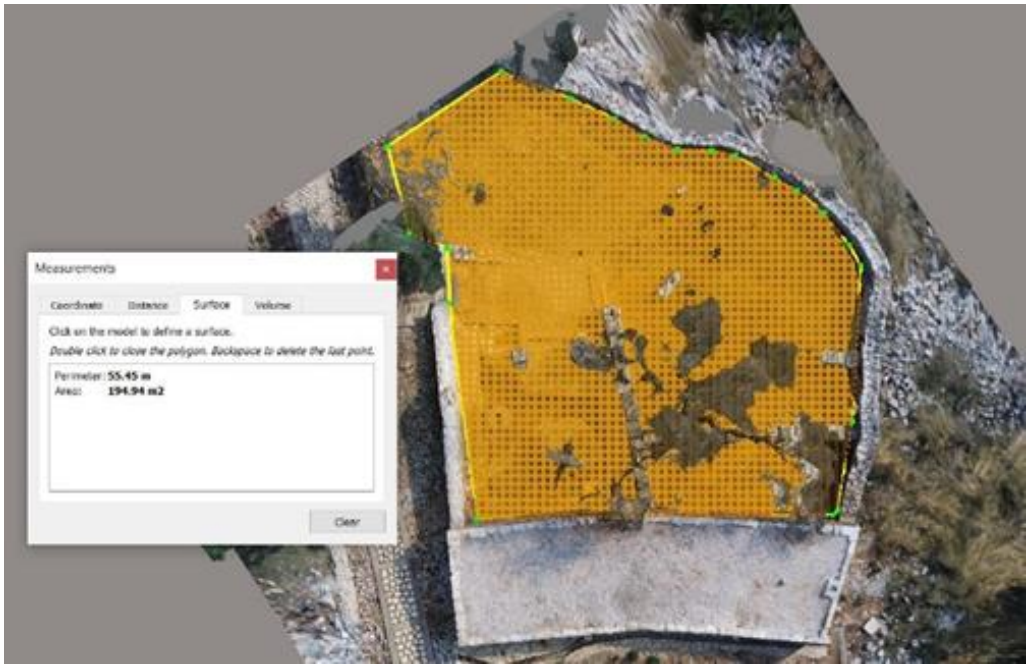

Figure 7. Garden area of the antique house

Figure 7 shows the garden area of the ancient house, which is about 195 m^2. Aside from that, the perimeter of the garden area was calculated as 55.45 meters. In order to calculate the usable garden area, the measurements were made from the inner border of the garden wall.

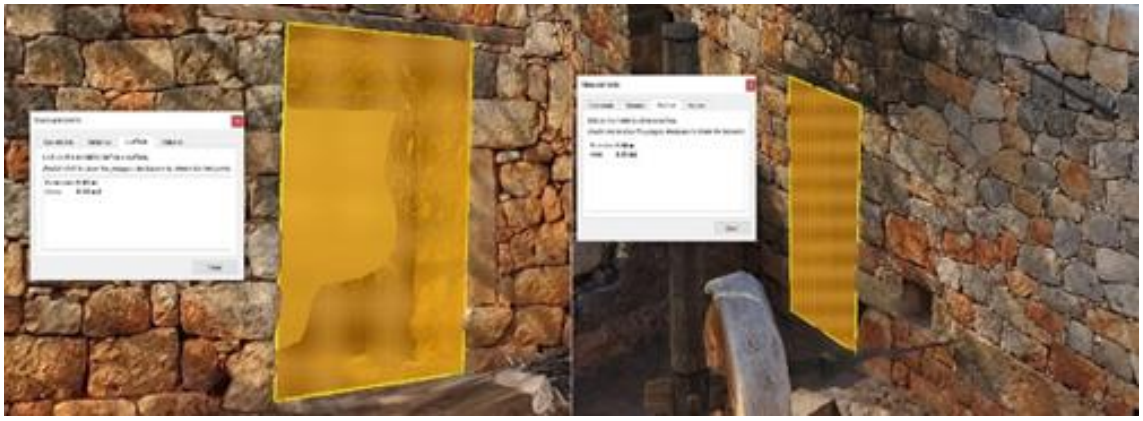

Figure 8. Measurements of building entrance doors

Figure 8 displays the measurements of the building entrance doors. There are 2 entrance doors to the building, and the first of these doors has an area of 2.11 square meters and the second one has an area of 1.85 square meters. The door on the side where the olive oil production workshop is located is the smaller one. There is a mechanism in the garden for olive oil production in the ancient village house and it covers an area of approximately 15.5 square meters.

In the last step of the study, the length and coordinate measurements of the models obtained with both software are presented comparatively in Table 3. The length and points used in the comparison are presented in the Figure 9 and 10.

Table 3 indicates the point coordinates acquired from Agisoft Metashape software. Table 4 shows the point coordinates obtained from Context Capture software. Table 5 and 6 presents the root mean square error (RMSE) calculations of the North and East coordinates. Table 7 indicates the RMSE calculation of the points' elevation values.

Figure 9. The points used in the comparison

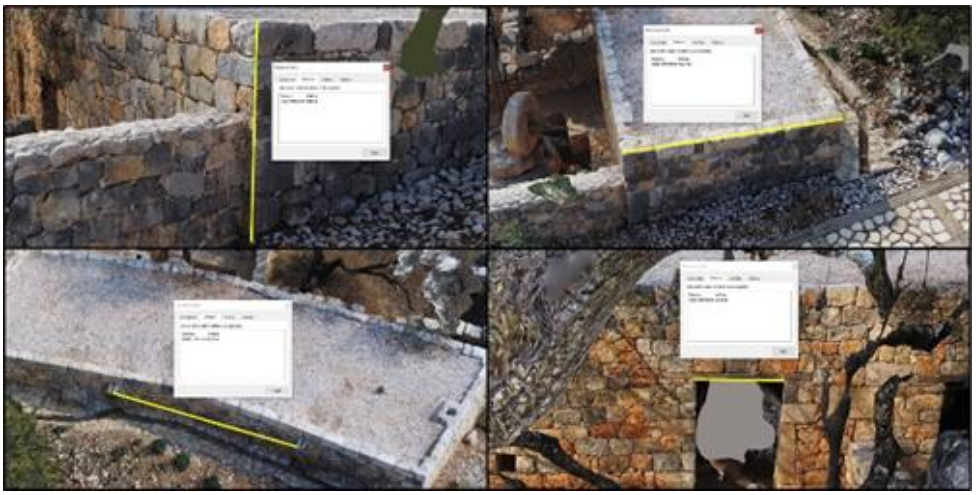

Figure 10. The lengths used in comparison

Table 3. The point coordinates (from Agisoft)

	North	East	Elevation
1	36.526776	34.177573	250.066
2	36.526881	34.177659	249.706
3	36.526898	34.177620	249.627
4	36.526805	34.177544	250.014
5	36.526810	34.177607	248.790
6	36.526834	34.177628	246.698
7	36.526865	34.177595	249.427
8	36.526828	34.177568	249.378

Table 4. The point coordinates (from Context Capture)

	North	East	Elevation
1	36.5267758	34.1775732	250.100
2	36.5268813	34.1776587	249.720
3	36.5268980	34.1776204	249.630
4	36.5268045	34.1775444	250.010
5	36.5268103	34.1776067	248.790
6	36.5268342	34.1776280	246.700
7	36.5268646	34.1775948	249.430
8	36.5268279	34.1775677	249.380

Table 5. RMSE calculation of the North coordinates [deg]

Agisoft	Context	Difference	Difference²
36.526776	36.5267758	2E-07	4E-14
36.526881	36.5268813	3E-07	9E-14
36.526898	36.5268980	0	0
36.526805	36.5268045	5E-07	2.5E-13
36.526810	36.5268103	3E-07	9E-14
36.526834	36.5268342	2E-07	4E-14
36.526865	36.5268646	4E-07	1.6E-13
36.526828	36.5268279	1E-07	1E-14
	RMSE		**2.91548E-07 deg**

Table 6. RMSE calculation of the East coordinates [deg]

Agisoft	Context	Difference	Difference²
34.177573	34.1775732	2E-07	4E-14
34.177659	34.1776587	3E-07	9E-14
34.177620	34.1776204	4E-07	1.6E-13
34.177544	34.1775444	4E-07	1.6E-13
34.177607	34.1776067	3E-07	9E-14
34.177628	34.1776280	0	0
34.177595	34.1775948	2E-07	4E-14
34.177568	34.1775677	3E-07	9E-14
	RMSE		**2.89396E-07 deg**

Table 7. RMSE calculation of the Z values [m]

Agisoft	Context	Difference	Difference²
250.066	250.100	0.034	0.001156
249.706	249.720	0.014	0.000196
249.627	249.630	0.003	9E-06
250.014	250.010	0.004	1.6E-05
248.790	248.790	0	0
246.698	246.700	0.002	4E-06
249.427	249.430	0.003	9E-06
249.378	249.380	0.002	4E-06
	RMSE		**0.0132 m**

Table 8. RMSE calculation of the lengths on the 3D solid models [m]

Agisoft	Context	Difference	Difference²
1.58	1.60	0.02	0.0004
3.93	3.93	0	0
4.92	4.90	0.02	0.0004
1.16	1.17	0.01	0.0001
0.92	0.92	0.0009	8.1E-07
1.88	1.88	0	0
6.31	6.30	0.01	1E-04
4.73	4.75	0.02	0.0004
	RMSE		**0.013233 m**

4. Discussion and Conclusion

When the obtained models are examined, although Context Capture gives better results visually, Agisoft gave better results in terms of mesh smoothness. According to Figures 6-7-8, it is seen that detailed measurements can be made on the models acquired. As a matter of fact, within the scope of this study, coordinate, length, area and volume measurements of the ancient house were conducted.

When it comes to consistency of results and comparison of software, the measurements made on the obtained models were examined. As indicated by Table 5-6, the consistency between the measured coordinate values is quite high because the RMSE value is low. Moreover, the fact that the RMSE values of the North and East coordinate data are almost the same among themselves strengthens the results.

As verified by Table 7, the elevation values of the points have a low RMSE value of 1.32 cm. For a building with a floor area of 52.16 square meters, the average error of 1.32 cm is considered to be at an acceptable level. When Table 8 is examined, the fact that the calculated difference value is the same as Table 7 reflects the consistency of the results in a way.

In a previously published and similar study, an ancient mausoleum was modeled and these analyzes were conducted [4]. In this study, the calculated difference value between both coordinate and length values was more

consistent than the previous study. The reason why the results are more consistent is thought to be the higher quality of the photo processing operation.

The high consistency of the results obtained with two different software proves the accuracy and usability of the models recreated. The 3D models received can be used in future studies such as restoration, modification and improvement. Furthermore, the 3D models acquired can be utilized by historians and archaeologists, as well as by local governments in advertising activities to improve tourism activities.

To summarize the study, digital documentation of an ancient village house located in the Ancient City of Olba in the Kanlıdivane region of Mersin province was carried out. Photogrammetric modeling was conducted by flying around the ancient village house via UAV. The modeling process was carried out with two separate software and the consistency of the results was presented comparatively. The fact that the calculated RMSE values were very small compared to the building size documented the consistency and usability of the results.

As a continuation of this research, it is planned to examine the thermal performance of the ancient village house.

Funding

This research received no external funding.

Author contributions

Engin Kanun: Conceptualization, Methodology, Software, Writing-Original draft **Aydın Alptekin:** Data curation, Writing-Original draft preparation, Software, Validation. **Lale Karataş:** Visualization, Investigation, Writing-Reviewing and Editing. **Murat Yakar:** Writing-Reviewing and Editing.

Conflicts of interest

The authors declare no conflicts of interest.

References

1. https://potamya.co/ilham/mezapotamya-mesos-potamos/
2. Ceylan, B. (2009). Kilikya'da Geç Antik dönem kirsal yerleşimleri: Kanytellis Örneği. *Olba*, (17), 35-62.
3. Kaplan, D., & Taşkiran, R. S. (2019). Olba Kaya Anıtlarında Mimari Cephe Tasarımları. *Seleucia*, (9), 181-203.
4. Kanun, E., Alptekin, A., & Yakar, M. (2021). Cultural heritage modelling using UAV photogrammetric methods: a case study of Kanlıdivane archeological site. *Advanced UAV*, *1*(1), 24-33.
5. Aydinoglu, U. (2015). Daglik Kilikia'da bir kirsal yerlesimin arkeolojisi. Ege Yayınları/Pitura. İstanbul.
6. Şimşek, A. (2011). Geçmişin nesnesini arayan bilim arkeoloji: Türkiye'de tarih öğretimindeki durumu. *Electronic Turkish Studies*, *6*(2), 919-934.
7. Çelik, M. Ö., Yakar, İ., Hamal, S., Oğuz, G. M., & Kanun, E. (2020). Sfm tekniği ile oluşturulan 3B modellerin kültürel mirasın belgelenmesi çalışmalarında kullanılması: Gözne Kalesi örneği. *Türkiye İnsansız Hava Araçları Dergisi*, *2*(1), 22-27.
8. Yakar, M., & Yilmaz, H. M. (2008). Kültürel miraslardan tarihi Horozluhan'in fotogrametrik rölöve çalişmasi ve 3 boyutlu modellenmesi. *Selçuk Üniversitesi Mühendislik, Bilim ve Teknoloji Dergisi*, *23*(2), 25-33.
9. Kanun, E., Metin, A., & Yakar, M. Yersel Lazer Tarama Tekniği Kullanarak Ağzıkara Han'ın 3 Boyutlu Nokta Bulutunun Elde Edilmesi. *Türkiye Lidar Dergisi*, *3*(2), 58-64.
10. Yakar, M., Yıldız, F., & Yılmaz, H. M. (2005). Tarihi Ve Kültürel Miraslarin Belgelenmesinde Jeodezi Fotogrametri Mühendislerinin Rolü. *TMMOB Harita ve Kadastro Mühendisleri Odası*, *10*.
11. Mirdan, O., & Yakar, M. (2017). Tarihi eserlerin İnsansız Hava Aracı ile modellenmesinde karşılaşılan sorunlar. *Geomatik*, *2*(3), 118-125.
12. Alptekin, A., & Yakar, M. (2021). 3D model of Üçayak Ruins obtained from point clouds. *Mersin Photogrammetry Journal*, *3*(2), 37-40.
13. Yakar, M., & Doğan, Y. (2017). Uzuncaburç Antik Kentinin İHA Kullanılarak Eğik Fotogrametri Yöntemiyle Üç Boyutlu Modellenmesi. 16. *Türkiye Harita Bilimsel ve Teknik Kurultayı. TMMOB Harita ve Kadastro Mühendisleri Odası, Ankara*.
14. Alptekin, A., Çelik, M. Ö., Doğan, Y., & Yakar, M. (2019). Mapping of a rockfall site with an unmanned aerial vehicle. *Mersin Photogrammetry Journal*, *1*(1), 12-16.

15. Alptekin, A., & Yakar, M. (2020). Heyelan bölgesinin İHA kullanarak modellenmesi. *Türkiye İnsansız Hava Araçları Dergisi*, *2*(1), 17-21.
16. Kusak, L., Unel, F. B., Alptekin, A., Celik, M. O., & Yakar, M. (2021). Apriori association rule and K-means clustering algorithms for interpretation of pre-event landslide areas and landslide inventory mapping. *Open Geosciences*, *13*(1), 1226-1244.
17. Alptekin, A., & Yakar, M. (2020). Determination of pond volume with using an unmanned aerial vehicle. *Mersin Photogrammetry Journal*, *2*(2), 59-63.
18. Ünel, F. B., Kuşak, L., Çelik, M., Alptekin, A., & Yakar, M. (2020). Kıyı çizgisinin belirlenerek mülkiyet durumunun incelenmesi. *Türkiye Arazi Yönetimi Dergisi*, *2*(1), 33-40.
19. Yılmaz, H. M., Aktan, N., Çolak, A., & Alptekin, A. (2022). Modelling Ozancık village (Aksaray) in computer environment using UAV photogrammetry. *Mersin Photogrammetry Journal*, *4*(1), 32-36.
20. Karataş, L., Alptekin, A., Kanun, E., & Yakar, M. (2022). Tarihi kârgir yapılarda taş malzeme bozulmalarının İHA fotogrametrisi kullanarak tespiti ve belgelenmesi: Mersin Kanlıdivane ören yeri vaka çalışması. *İçel Dergisi*, *2*(2), 41-49.

Advanced UAV
http://publish.mersin.edu.tr/index.php/uav
e-ISSN 2822-6976

Detection and documentation of stone material deterioration in historical masonry structures using UAV photogrammetry: A case study of Mersin Aba Mausoleum

Lale Karataş [*1], Aydın Alptekin [2], Murat Yakar [3]

[1]*Mardin Artuklu University, Department of Architecture and Urban Planning, Mardin, Türkiye, lalekaratas@artuklu.edu.tr*
[2]*Mersin University, Department of Geological Engineering, Mersin, Türkiye, aydinalptekin@mersin.edu.tr*
[3]*Mersin University, Geomatics Engineering Department, Mersin, Türkiye, myakar@mersin.edu.tr*

Cite this study: Karataş, L., Alptekin, A., & Yakar, M. (2022). Detection and documentation of stone material deterioration in historical masonry structures using UAV photogrammetry: A case study of Mersin Aba Mausoleum. Advanced UAV, 2 (2), 51-64

Keywords
Cultural Heritage
UAV Photogrammetry
Stone material
Material problems
Sustainability

Research Article
Received: 04.10.2022
Revised: 08.11.2022
Accepted: 18.11.2022
Published: 30.11.2022

Abstract

The Aba mausoleum, located in the ancient city of Mersin Kanlıdivane, is one of the most well-known places in the region. Although the architectural integrity of the building is partially preserved, material deterioration and structural deformations are observed especially on the west and north walls. Since the monument is one of the few examples of architectural and structural integrity that still exists, it should be included in the architectural preservation program as soon as possible before it loses its structural integrity. Accurate identification of the causes and types of degradation is of great importance in designing conservation interventions. In this study, it is aimed to detect and document the stone material deterioration of Mersin Aba mausoleum, which is a great necessity for the sustainability of cultural heritage, by using UAV photogrammetry. UAV photogrammetry and mapping techniques were used as a method in the study. The data obtained as a result of the study show that, thanks to their high resolution, a deterioration map can be created for the detection of material deterioration and restoration analysis quickly and easily. In addition, as a result of the study, it is seen that the most common types of stone material deterioration in the building are surface pollution, cracks and exfoliation. According to this result, it is seen that even the types of material problems based on the smallest detail can be determined based on virtual visual inspection, thanks to UAV photogrammetry, without observing the structure on-site with UAVs.

1. Introduction

A large percentage of the world's tangible cultural heritage is made of stone, and stone monuments are slowly but irreversibly disappearing. For example, it has been calculated that limestone will erode an average of 1.5-3 mm of rock within 100 years in temperate climates and will cause the loss of inscriptions on tombstones in the United Kingdom within 300 years [1]. When the causes of material deterioration in historical stone structures are examined, it is seen that the most common cause of material deterioration in stone structures in the world is caused by natural environmental factors or human-induced reasons. For example, rain water, which is a natural environmental factor, penetrates into the stone and accelerates the freezing/thawing cycles and dissolution processes of the stone. In addition, pollutants in the air can be carried into the stone by rain water and can play an important role in the deterioration of the stone, as it accelerates the formation of a black crust called surface pollution by chemical decomposition of the stone [2]. Rands et al. [3] found that both acidity and ionic strength in rainwater play an important role in limestone degradation. Butlin et al. [4] show that sulfur dioxide makes a

significant contribution to the degradation of calcareous stones in high pollution areas and is a major cause of stone dissolution, particularly in the United Kingdom. The types of material degradation caused by these causes are seen in many different types, including cracking, blistering, surface loss, fragmentation, discoloration, biodegradation and damage from previous intervention [5-16].

Different new technologies have been developed in surveying of architectural documentation. Digital photogrammetry, 3D Laser Scanning and UAV are some of the surveying Technologies of cultural heritages. The development of digital photogrammetry to use cultural heritage is provided simplicity on the works carried out either on the field or on the laboratory. As a result of this development, the application of the photogrammetry science on the various topics is increased its application to be used much more effectively [17-20].

The use of three-dimensional computer graphics and visualization techniques is becoming more and more popular, because these techniques visualize more realistic object models than graphic based object models [21-27].

The other modern technology of measurement of cultural heritages is laser 3D laser scanning. Laser Scanning is a non-contact, technology that digitally captures the shape of physical objects using laser light. 3D laser scanners create “point clouds” of data from the surface of an object [28-33].

Using of unmanned aerial vehicles (UAVs) are becoming more effective tools for researchers for their applications. unmanned aerial vehicle is a very beneficial tool to obtain information without touching the object. [34-38].

For the treatment of material deterioration seen on the facades of historical buildings, first of all, the types of deterioration must be correctly identified. In some cases, it is possible to solve the deterioration of stone structures without touching the structures, only by improving the environmental conditions. In this context, it is very important to correctly diagnose the cause of deterioration in stone material [39]. Mapping the deterioration of facades in urban historical contexts represents a preliminary activity for the preparation of any restoration project [2]. However, the creation of deterioration maps of facades by manual methods is time consuming and laborious.

In the literature, it is seen that terrestrial laser scanning, photogrammetry and also unmanned aerial vehicles called "drones" are used in the creation of material deterioration maps of facades. The use of digital tools to support mapping activities has resulted in more detailed results on facade analysis, leading to simplification of its operations [40]. Surveys based on terrestrial laser scanning (TLS) tools in the literature yield very good geometric data in terms of high resolution, high accuracy and low uncertainty, but often yield dense point clouds that are not useful for disturbance mapping. Because color data is not always reliable in TLS data, this shortcoming is partially compensated by adding an external high-performance digital camera or collecting large numbers of photos to create high resolution (HDR) images [41]. In addition, the data obtained from TLS is limited to the camera angle [42] and it is considered to be relatively difficult to access due to the expensiveness of the instruments used [43]. In addition, site conditions and obstructions caused by different types of objects (for example, structural components that cause self-shadowing) in historical buildings may make the application of this technique insufficient for general research. It is seen that terrestrial laser scanning or terrestrial photogrammetry applications do not give satisfactory results in this case, since the deterioration mapping of facades is difficult in historical urban contexts, which are often characterized by narrow streets and tall buildings. In the researches, it is emphasized that the use of UAV photogrammetry in the deformation maps of the facades has several advantages over terrestrial laser scanning and photogrammetry methods. The common emphasis in these studies is that the use of UAVs equipped with commercial cameras leads to lower vehicle cost, higher data collection speed, and most importantly, better representation of materials and material issues [44-46]. In addition, the use of UAV photogrammetry is low cost, fast and easy to use compared to terrestrial laser scanning [2]. In the studies, it is stated that the UAV photogrammetry method is also the best solution to overcome the terrain limitations and to investigate the facade areas that are hidden from the ground or inaccessible [47].

In many studies, it has been found that it is easily possible to model buildings from close range or to monitor material deterioration using UAVs [48-51]. Russo et al. [2] used UAV photogrammetry to analyze the facade of a large historic building in Bologna (Italy), and as a result of the study, geometric data as well as material information useful for architectural analysis and restoration planning were obtained. The results of the study show that with the drone it is possible to obtain a metric orthophoto image of the facade of a historic building of suitable quality for a detailed mapping of stone material degradation. In addition, the obtained data showed that, thanks to their high resolution, a deterioration map can be generated quickly and easily to support restoration analysis. Cavalagli et al. [51] conducted photogrammetric research with drones to create a 3D model and damage maps of a historic stone arch bridge located in the ancient Via Amerina (Todi, Perugia, Italy). As a result of the study, it was determined that the assessment of structural damage by photogrammetric research with UAVs and especially cracks, microcracks and material shortages can be mapped without direct access and this can be done based on virtual visual inspection. In addition, in the study, the point cloud obtained by UAV photogrammetric research was compared with a point cloud based on the TLS survey, as a result, it was shown that the UAV-based research method provides more material resolution than the TLS method and can provide significant advantages by reducing the working time. In the application to a severely damaged historical structure, the study showed that the use of UAV-based photogrammetry can provide a detailed detection of all types of material deterioration,

including surface loss and significant cracks in the structure, and is very effective in quickly highlighting damage and estimating missing material volumes. Such a methodology has proven to be very effective for the investigation of inaccessible structures and for the quantitative estimation of damage to historic masonry structures.

Although the architectural integrity of the Aba mausoleum in Mersin Kanlıdivane Ancient City is partially preserved, material deteriorations and structural deformations are observed especially on the west and north walls. Accurate identification of the causes and types of degradation is of great importance in designing conservation interventions. In this study, it is aimed to detect and document the stone material deterioration of Mersin Aba mausoleum, which is a great necessity for the sustainability of cultural heritage, by using UAV photogrammetry.

2. Study Area

The Aba Mausoleum, an ancient monument built in the 2nd century AD in the Kanlıdivane Region of Mersin province of Turkey, has coordinates 36°31'38.5"north, 34°10'37.4" east (Figure 1). This structure, built in the type of Roman temples, is the most magnificent mausoleum in the ancient city. According to the inscription on the door of the mausoleum, it was built by a woman named Aba for herself and her husband Arios. Based on the inscription and other tombs on it, the tomb is dated to the 2nd century AD. The Aba Mausoleum is located to the north of the geological pit in the region and is one of the best-known places in Kanlıdivane.

The tomb monument is built on a low podium, has a vaulted entrance on the front and has Corinthian plaster capitals on its four corners. The building was built with the masonry technique and was built of cut stone. Mortar was used as the binding material. The roof of the superstructure is in the form of a cradle and is stone paved. The last row of cut stones on the masonry walls was built in the architrave style, and the cornerstones were made in the Corinthian capital style [52].

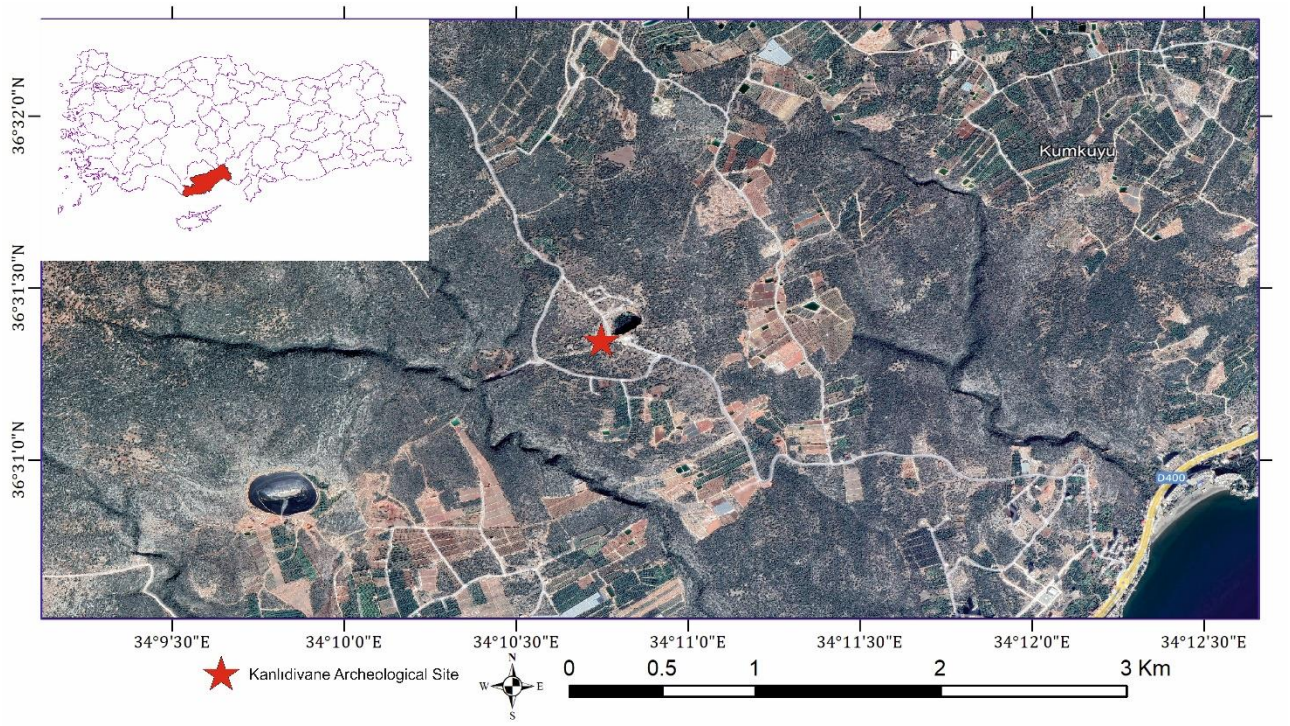

Figure 1. Location map of the study area

3. Method

In the first stage, the process of taking images of the mausoleum with an unmanned aerial vehicle was carried out. At this stage of the study, first of all, the necessary permissions for the flight were obtained. Images were taken manually with Parrot Anafi HDR drone around the tomb in the Kanlıdivane region (Figure 2).

In the second stage, the data taken from the unmanned aerial vehicle was transferred to the computer environment. Material deteriorations were examined from the images obtained, and they were processed on the chart prepared on the basis of classification of building elements. Based on the information in the chart prepared at the last stage, mapping was performed on the images and material deterioration was defined (Table 1).

Figure 2. Anafi Parrot

Table 1. Properties of drone

Feature	Value
Drone	
Size folded	244x67x65 mm
Size unfolded	175x240x65 mm
Weight	320 g
Max transmission range	4km with controller
Max flight time	25 min
Max horizontal speed	15 m/s
Max vertical speed	4 m/s
Max wind resistance	50 km/h
Service ceiling	4500m above sea level
Operating temperature	-10°C to 40°C
Lens	
Sensor	1/2.4'' CMOS
Aperture	f/2.4
Focal length (35 mm eq.)	23-69 mm (photo)
Depth of field	1.5 m - ∞
ISO range	100-3200
Digital zoom	up to 3x (4K Cinema, 4K UHD, FHD)
Photo resolution	21MP (5344x4016) / 4:3 / 84° HFOV

Table 2. Stone material deterioration on the facades of the monumental tomb structure

NATURAL STONE CONSTRUCTION ELEMENTS			PROBLEMS ENCOUNTERED ON CONSTRUCTION ELEMENTS MADE OF MASONRY MATERIAL IN BURDUR GAR																			Faulty Repairs		
			Loss of surface	Fragmentation	Formation of gap/ hole	Pitting	Cracks	Exfoliation	Foliation	Discharge of jointing	Surface contamination	Shell formation	Efflorescence	Crystallization	Formation of plant	Formation of moss	Corrosion (Rust stain)	Tear	Loss of form	Colour change	Use of cement	Fall of plaster	Other
VERTICAL BEARINGS	SINGLE BEARINGS	Leg	-	-	-	-	-	-	-	-	-	-	-	-	-	-	-	-	-	-	-	-	-
		Column	-	-	-	-	-	-	-	-	-	-	-	-	-	-	-	-	-	-	-	-	-
	CONTINUOUS BEARINGS	Wall	X	-	-	-	X	-	-	-	X	-	-	-	X	-	-	-	-	-	X	X	X
HORIZONTAL BEARINGS	FLOORINGS	Flat	-	-	-	-	-	-	-	-	-	-	-	-	-	-	-	-	-	-	-	-	-
			-	-	-	-	-	-	-	-	-	-	-	-	-	-	-	-	-	-	-	-	-
		Curvilinear																					
WALL OPENINGS	Window	Lintel / jamb	-	-	-	-	-	-	-	-	-	-	-	-	-	-	-	-	-	-	-	-	-
		Sill	-	-	-	-	-	-	-	-	-	-	-	-	-	-	-	-	-	-	-	-	-
	Door	Lintel / jamb	-	-	-	-	-	-	-	-	-	-	-	-	-	-	-	-	-	-	-	-	-
		Sill	-	-	-	-	-	-	-	-	-	-	-	-	-	-	-	-	-	-	-	-	-
	Arch		-	-	-	-	-	-	-	-	-	-	-	-	-	-	-	-	-	-	-	-	-
AUXILIARY ELEMENTS	Network		X	-	-	-	-	-	-	-	-	-	-	-	X	-	-	-	-	-	-	-	-
	Moulding																						
	Gargoyle																						
	Chimney																						
	Element for passage to the cover																						

4. Results

Based on the information in the chart prepared at the last stage, mapping was performed on the images and material deterioration was defined.

4.1. Material Deterioration in Single Carriers

In masonry structures, the only carriers are legs and columns. There are two pillars used in the building. The problems seen in the feet that make up the structure are in the form of scaling and color change caused by the effect of rain.

Figure 3. Scaling and discoloration of the feet

3.2. Material Deterioration in Continuous Carriers

In masonry structures, the continuous carriers are the walls. Material deteriorations on the walls were determined as surface loss, joint discharge, plant formations, and surface pollution. It has been determined that the rain water on the walls of the building causes material losses (surface loss) on the calcareous stone surface intensively as a result of the penetration of the rain water into the inner structure of the calcareous stone and its sudden evaporation due to sudden temperature increases in the geographical context. Rain water also caused the local mortar between the walls to melt, causing joint discharges. Plant formations are seen in these areas as a result of factors such as wind and various living things carrying plant seeds between the joints with the emptying of the joint spaces. In addition, there is an intense surface pollution caused by human-induced causes in the building. In order to destroy the bushes in the ancient city, the stubble burning processes in the immediate vicinity of the building, which the surrounding people removed, showed itself as a black layer on the stone material. In addition, there are serious cracks in the wall that divide the stone components into two. This graph shows a high probability of impact triggered by lateral thrusts or seating issues. As the monument is located very close to one of the geological discontinuity lines of the site, the danger of structural deterioration is confirmed by external forces.

It has been determined that the structural body wall forming the south façade of the building is in the form of exfoliation, joint discharge, surface loss, surface pollution caused by human effects, crusting and fragmentation caused by the effect of rain (Figure 6).

On the eastern façade of the building, surface pollution caused by human-induced effects, joint discharge, plant formation, gap hole formation, surface loss and color change can be seen as a result of the effect of rain water on the stone. In addition, there are serious cracks in the wall that divide the stone components into two. This graph shows a high probability of impact triggered by lateral thrusts or seating issues (Figure 7).

On the northern body wall of the building, there are serious cracks triggered by human-induced surface pollution, fragment rupture, joint discharge caused by rain, and lateral pressures or settlement problems (Figure 8).

On the eastern façade of the building, joint discharge, fragmentation, surface pollution, exfoliation and loss of surface stone material problems are observed (Figure 9).

exfoliation (a)

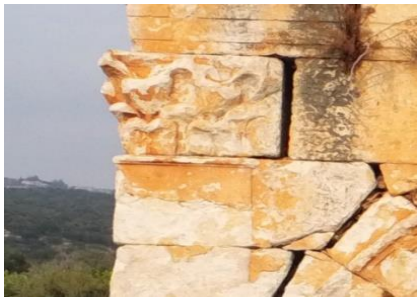

Joint discharge(b)

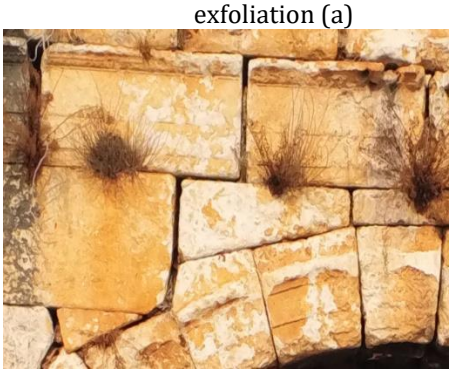

Plant (c)

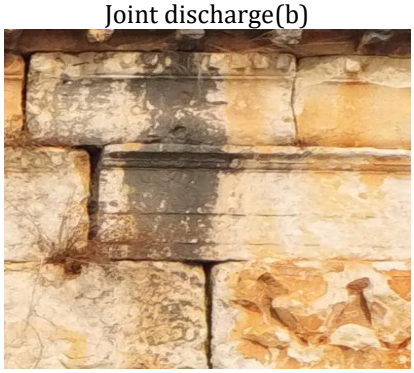

Surface contamination (d)

Soil crust(e)

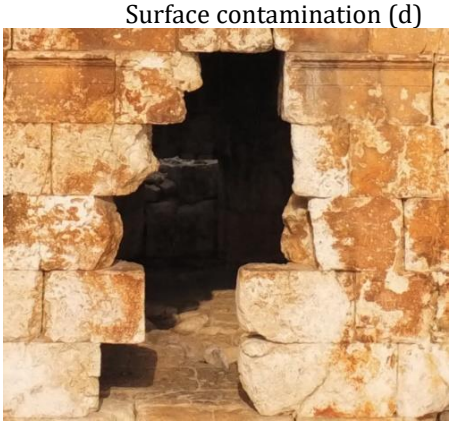

Chunking (f)

Figure 4. Material Deterioration on the Southern Front

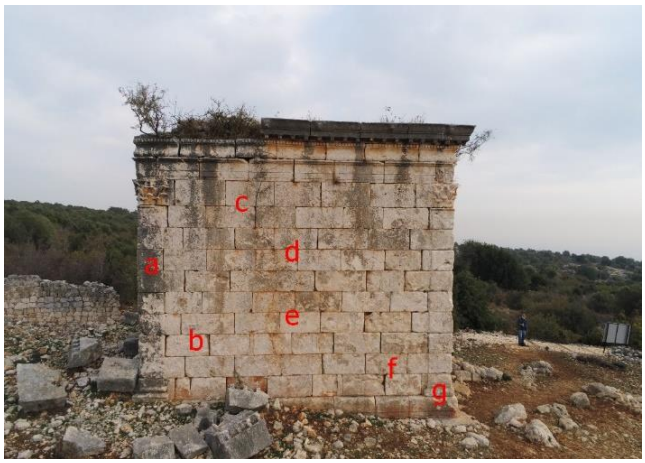

(a) Surface contamination

(b) Joint discharge

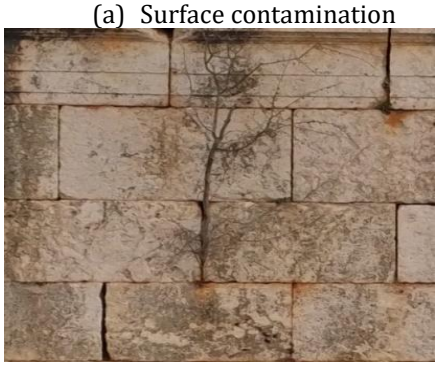

(c) Plant

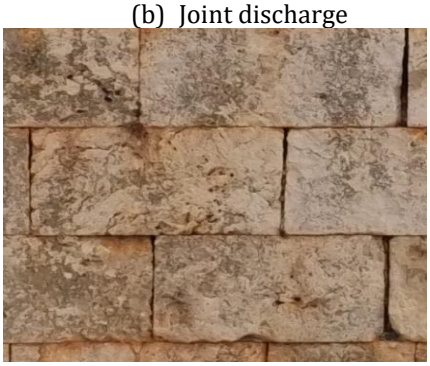

(d) Void-hole Formation

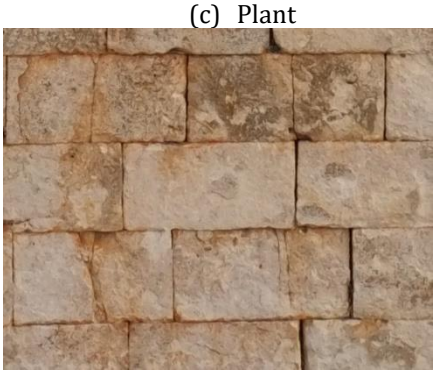

(e) fracture

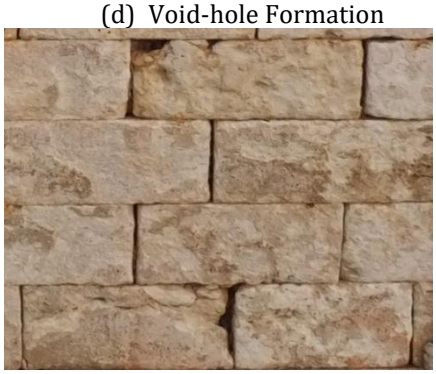

(f) Surface loss

(g) Color change

Figure 5. Material Deterioration on the Eastern Front

(a) Surface contamination

(C) fragment rupture

(b) Fracture

(d) Joint Discharge

Figure 6. Material Deterioration on the Northern Front

(a) Joint Discharge

(b) fragment rupture

(c) Surface contamination

(d) exfoliation

(e) surface loss

Figure 7. Material Deterioration on the Eastern Front

3.3. Material Deterioration in Horizontal Carriers

In masonry structures, horizontal carriers are floors. Plant formations originating from the effect of water can be seen on the flat floor seen in the building (Figure 10).

Figure 8. Plant formation seen on the floor

3.4. Material Deterioration in Wall Cavities

The structural elements that make up the wall spaces in masonry structures are arches. The discoloration of the arches as a result of the joint discharge of the rain and the effect of the sun can be seen (Figure 11).

Figure 9. Joint discharge and discoloration in the arch

3.5. Material Deterioration in Auxiliary Elements

Building elements that make up auxiliary elements in masonry structures are moldings, ornaments and muqarnas. Surface pollution caused by human influence is observed in the wipes. Moisture-based plant formations were observed in places. On the other hand, it was determined that there were color changes in the decorations due to the effect of the sun (Figure 12).

Surface pollution in wipes, Plant formation

Color change in ornament

Surface pollution in decoration

Figure 10. Stone material deterioration in auxiliary elements

5. Discussion

In the study, it was aimed to detect and document the stone material deterioration of Mersin Aba mausoleum, which is a great necessity for the sustainability of cultural heritage, by using UAV photogrammetry. In the study, a deterioration map could be generated from the data obtained by UAV photogrammetry to support restoration analysis quickly and easily, thanks to their high resolution. According to this result, it is seen that the UAV photogrammetry method can provide images with sufficient resolution for the detection of material deterioration of stone structures. This result supports the fact that it is easily possible to model buildings from close range or to control material deterioration using UAVs obtained in various studies in the literature [48-51].

In addition, with this method, it has been achieved that it provides a higher data collection rate than the traditional method and provides a better representation of the material and material problems. This result supports the fact that the use of UAVs equipped with commercial cameras obtained in various studies in the literature provides lower vehicle cost, higher data collection speed, and most importantly, a better representation of materials and material problems [44-46].

Another finding is that the material problems can be easily detected from the images obtained with the unmanned aerial vehicle without examining the structure in the field. Remondino et al. [47] and Cavalagli et al. [51] found that UAV photogrammetry is also one of the best solutions to overcome terrain limitations and investigate facade areas that are hidden or inaccessible from the ground, and that such a methodology can be used to investigate inaccessible structures and damage historical masonry structures and supports the conclusion that it is very effective for quantitative estimation.

Another important finding was that as a result of the study, images of the facades were obtained in orthophoto to investigate the material deteriorations on the facade and the deteriorations on the facade could be mapped. This finding supports the conclusion of Russo et al. [2] that it is possible to obtain a metric orthophoto image of the facade of a historic building of suitable quality for a detailed mapping of stone material deterioration on the facades.

Another finding was that the most common stone material deterioration types in the building were surface pollution, cracks and exfoliation. According to this result, it is seen that the assessment of structural damage by photogrammetric research with UAVs and especially cracks, microcracks and material shortages can be mapped

without direct access, and this can be done based on virtual visual inspection. This result supports the results obtained by Cavalagli et al. [51], that even the types of material problems can be determined based on the smallest detail, based on virtual visual inspection only, thanks to UAV photogrammetry, without examining the structure in situ with UAVs.

6. Conclusion

The Aba mausoleum, located in the ancient city of Mersin Kanlıdivane is one of the most well-known places in the region. The data obtained in the results of the study showed that, thanks to their high resolution, a deterioration map can be created quickly and easily to support restoration analysis.

Although the architectural integrity of the building was partially preserved in the findings obtained as a result of the study, it was observed that there were material deteriorations and structural deformations, especially on the west and north walls. There are serious cracks in the north wall that divide the stone components into two. This indicates a high probability of impact triggered by lateral thrusts or settlement issues. Since the monument is one of the few examples of architectural and structural integrity that still exists, it should be included in the architectural preservation program as soon as possible before it loses its structural integrity.

Funding

This research received no external funding.

Author contributions

Lale Karataş; Methodology, data collection, writing **Aydın Alptekin;** Writing, Control. **Murat Yakar:** Editing the manuscript

Conflicts of interest

The authors declare no conflicts of interest.

References

1. Allsopp, D., & Gaylarde, C. C. (2004). Heritage Biocare. Training course notes in Biodeterioration for Museums, Libraries, Archives and Cultural Properties, version 2.
2. Russo, M., Carnevali, L., Russo, V., Savastano, D., & Taddia, Y. (2019). Modeling and deterioration mapping of façades in historical urban context by close-range ultra-lightweight UAVs photogrammetry. *International journal of architectural heritage*, *13*(4), 549-568.
3. Rands, D. G., Rosenow, J. A., & Laughlin, J. S. (1986). Effects of acid rain on deterioration of coquina at Castillo de San Marcos National Monument. Materials Degradation Caused by Acid Rain, 318, 307-310.
4. Butlin, R. N., Coote, A. T., Devenish, M., Hughes, I. S. C., Hutchens, C. M., Irwin, J. G., ... & Yates, T. J. S. (1992). Preliminary results from the analysis of stone tablets from the National Materials Exposure Programme (NMEP). *Atmospheric Environment. Part B. Urban Atmosphere*, *26*(2), 189-198.
5. Normal, R. (1990). 1/88: Alterazioni macroscopiche dei materiali lapidei: Lessico. *CNRICR, Roma*.
6. Franke, L., Schumann, I., Van Hees, R., Van der Klugt, L. J. A. R., Naldini, S., Binda, L., ... & Mateus, J. (1998). *Damage Atlas, Classification of damage patterns found in brick masonry*. Frauenhofer IRB Verlag; Stuttgart.
7. Henriques, F. M. A., Rodrigues, J. D., Aires-Barros, L., & Proença, N. (2005). Materiais pétreos e similares–Terminologia das formas de alteração e degradação. *LNEC, Lisboa, Portugal*.
8. Fitzner, B., Heinrichs, K., & Kownatzki, R. (1995). *Weathering Forms, Classification and Mapping: Verwitterungsformen-Klassifizierung und Kartierung*. Ernst and Sohn.
9. Fitzner, B. (2002, May). Damage diagnosis on stone monuments-in situ investigation and laboratory studies. In *Proceedings of the International Symposium of the Conservation of the Bangudae Petroglyph* (Vol. 7, pp. 29-71). Seoul, Korea: Seoul National University.
10. Jo, Y. H., & Lee, C. H. (2014). Quantitative modeling of blistering zones by active thermography for deterioration evaluation of stone monuments. *Journal of Cultural Heritage*, *15*(6), 621-627.
11. Cutler, N. A., Viles, H. A., Ahmad, S., McCabe, S., & Smith, B. J. (2013). Algal 'greening'and the conservation of stone heritage structures. *Science of the Total Environment*, *442*, 152-164.

12. Adamopoulos, E., & Rinaudo, F. (2021). Combining multiband imaging, photogrammetric techniques, and FOSS GIS for affordable degradation mapping of stone monuments. *Buildings*, *11*(7), 304.
13. Patil, S. M., Kasthurba, A. K., & Patil, M. V. (2021). Characterization and assessment of stone deterioration on heritage buildings. *Case Studies in Construction Materials*, *15*, e00696.
14. Kramar, S., Mladenović, A., Pristacz, H., & Mirtič, B. (2011). Deterioration of the black Drenov Grič limestone on historical monuments (Ljubljana, Slovenia). *Acta Carsologica*, *40*(3).
15. Bozdağ, A., İnce, İ., Bozdağ, A., Hatır, M. E., Tosunlar, M. B., & Korkanç, M. (2020). An assessment of deterioration in cultural heritage: The unique case of Eflatunpınar Hittite Water Monument in Konya, Turkey. *Bulletin of Engineering Geology and the Environment*, *79*(3), 1185-1197.
16. Rodrigues, J. D. (2015). Defining, mapping and assessing deterioration patterns in stone conservation projects. *Journal of Cultural Heritage*, *16*(3), 267-275.
17. Yakar, M., Kabadayı, A., Yiğit, A. Y., Çıkıkcı, K., Kaya, Y., & Catin, S. S. (2016). Emir Saltuk Kümbeti fotogrametrik rölöve çalişmasi ve 3boyutlu modellenmesi. *Geomatik*, *1*(1), 14-18.
18. Ulvi, A., Yakar, M., Alyilmaz, C., & Alyilmaz, S. (2017). Using the close range photogrammetry technique in 3-dimensional work: History of obrukhan sample. *International Multidisciplinary Scientific GeoConference: SGEM*, *17*, 347-355.
19. Alyilmaz, C., Alyilmaz, S., & Yakar, M. (2010). Measurement of petroglyhps (rock of arts) of Qobustan with close range photogrammetry. *International Archives of Photogrammetry, Remote Sensing and Spatial Information Sciences*, *38*(Part 5), 29-32.
20. Yakar, M., & Doğan, Y. (2017). Mersin Silifke Mezgit Kale Anıt Mezarı Fotogrametrik Rölöve Alımı Ve Üç Boyutlu Modelleme Çalışması. *Geomatik*, *2*(1), 11-17.
21. Yilmaz, H. M., Yakar, M., & Yildiz, F. (2008). Digital photogrammetry in obtaining of 3D model data of irregular small objects. *The International Archives of the Photogrammetry, Remote Sensing and Spatial Information Sciences*, *37*, 125-130.
22. Unal, M., Yakar, M., & Yildiz, F. (2004, July). Discontinuity surface roughness measurement techniques and the evaluation of digital photogrammetric method. In *Proceedings of the 20th international congress for photogrammetry and remote sensing, ISPRS* (Vol. 1103, p. 1108).
23. Yakar, M. (2009). Digital elevation model generation by robotic total station instrument. *Experimental Techniques*, *33*(2), 52-59.
24. Yakar, M., & Doğan, Y. (2018). Gis and three-dimensional modeling for cultural heritages. *International Journal of Engineering and Geosciences (IJEG)*, *3*(2), 50-55.
25. Yakar, M., Yılmaz, H. M., & Mutluoğlu, Ö. (2010). Close range photogrammetry and robotic total station in volume calculation International Journal of the Physical Sciences, 5 (2), 86-96.
26. Yilmaz, H. M., Yakar, M., Mutluoglu, O., Kavurmaci, M. M., & Yurt, K. (2012). Monitoring of soil erosion in Cappadocia region (Selime-Aksaray-Turkey). *Environmental Earth Sciences*, *66*(1), 75-81.
27. Korumaz, A. G., Dülgerler, O. N., & Yakar, M. (2011). Kültürel mirasin belgelenmesinde dijital yaklaşimlar. *Selçuk Üniversitesi Mühendislik, Bilim ve Teknoloji Dergisi*, *26*(3), 67-83.
28. Alptekin, A., Fidan, Ş., Karabacak, A., Çelik, M. Ö., & Yakar, M. (2019). Üçayak Örenyeri'nin yersel lazer tarayıcı kullanılarak modellenmesi. *Türkiye Lidar Dergisi*, *1*(1), 16-20.
29. Alptekin, A., & Yakar, M. (2021). 3D model of Üçayak Ruins obtained from point clouds. *Mersin Photogrammetry Journal*, *3*(2), 37-40.
30. Yilmaz, H. M., & Yakar, M. (2006). Yersel lazer tarama Teknolojisi. *Yapı teknolojileri Elektronik dergisi*, *2*(2), 43-48.
31. Yakar, M., Yilmaz, H. M., & Mutluoglu, O. (2014). Performance of Photogrammetric and Terrestrial Laser Scanning Methods in Volume Computing of Excavtion and Filling Areas. *Arabian Journal for Science and Engineering*, *39*(1), 387-394.
32. Yakar, M., Yılmaz, H. M., & Mutluoğlu, H. M. (2009). Hacim Hesaplamalarında Laser Tarama ve Yersel Fotogrametrinin Kullanılması, TMMOB Harita ve Kadastro Mühendisleri Odası 12. *Türkiye Harita Bilimsel ve Teknik Kurultayı, Ankara*.
33. Yakar, M., & Yilmaz, H. M. (2011). Determination of erosion on a small fairy chimney. *Experimental Techniques*, *35*(5), 76-81.
34. Kanun, E., Alptekin, A., & Yakar, M. (2021). Cultural heritage modelling using UAV photogrammetric methods: a case study of Kanlıdivane archeological site. *Advanced UAV*, *1*(1), 24-33.
35. Ulvi, A., Yakar, M., Yiğit, A. Y., & Kaya, Y. (2020). İHA ve yersel fotogrametrik teknikler kullanarak Aksaray Kızıl Kilise'nin 3 Boyutlu nokta bulutu ve modelinin üretilmesi. *Geomatik Dergisi*, *5*(1), 22-30.
36. Mırdan, O. & Yakar, M. (2017). Tarihi Eserlerin İnsansız Hava Aracı İle Modellenmesinde Karşılaşılan Sorunlar. Geomatik, 2 (3), 118-125.
37. Karataş, L., Alptekin, A., Kanun, E., & Yakar, M. (2022). Tarihi kârgir yapılarda taş malzeme bozulmalarının İHA fotogrametrisi kullanarak tespiti ve belgelenmesi: Mersin Kanlıdivane ören yeri vaka çalışması. *İçel Dergisi*, *2*(2), 41-49.

38. Alptekin, A., & Yakar, M. (2020). Heyelan bölgesinin İHA kullanarak modellenmesi. *Türkiye İnsansız Hava Araçları Dergisi*, *2*(1), 17-21.
39. Smith, B. J., Baptista-Neto, J. A., Silva, M. A. M., McAlister, J. J., Warke, P. A., & Curran, J. M. (2004). The decay of coastal forts in southeast Brazil and its implications for the conservation of colonial built heritage. *Environmental Geology*, *46*(3), 493-503.
40. Del Pozo, S., Herrero-Pascual, J., Felipe-García, B., Hernández-López, D., Rodríguez-Gonzálvez, P., & González-Aguilera, D. (2016). Multispectral radiometric analysis of façades to detect pathologies from active and passive remote sensing. *Remote Sensing*, *8*(1), 80.
41. Russo, M., & Manferdini, A. M. (2014). Integration of image and range-based techniques for surveying complex architectures. *ISPRS Annals of the Photogrammetry, Remote Sensing and Spatial Information Sciences*, *2*(5), 305.
42. Soudarissanane, S., Lindenbergh, R., Menenti, M., & Teunissen, P. (2011). Scanning geometry: Influencing factor on the quality of terrestrial laser scanning points. *ISPRS journal of photogrammetry and remote sensing*, *66*(4), 389-399.
43. Chen, S., Laefer, D. F., Mangina, E., Zolanvari, S. I., & Byrne, J. (2019). UAV bridge inspection through evaluated 3D reconstructions. *Journal of Bridge Engineering*, *24*(4), 05019001.
44. Achille, C., Adami, A., Chiarini, S., Cremonesi, S., Fassi, F., Fregonese, L., & Taffurelli, L. (2015). UAV-based photogrammetry and integrated technologies for architectural applications—methodological strategies for the after-quake survey of vertical structures in Mantua (Italy). *Sensors*, *15*(7), 15520-15539.
45. Khaloo, A., Lattanzi, D., Jachimowicz, A., & Devaney, C. (2018). Utilizing UAV and 3D computer vision for visual inspection of a large gravity dam. *Frontiers in Built Environment*, 31.
46. Barba, S., Barbarella, M., Di Benedetto, A., Fiani, M., Gujski, L., & Limongiello, M. (2019). Accuracy assessment of 3D photogrammetric models from an unmanned aerial vehicle. *Drones*, *3*(4), 79.
47. Remondino, F., Spera, M. G., Nocerino, E., Menna, F., & Nex, F. (2014). State of the art in high density image matching. *The photogrammetric record*, *29*(146), 144-166.
48. Caroti, G., I. Martınez-Espejo Zaragoza, A. & Piemonte (2015). Accuracy assessment in structure from motion 3D reconstruction from UAV-born images: The influence of the data processing methods. International Archives of Photogrammetry, Remote Sensing and Spatial Information Sciences XL-1/W4 (1), 103–109.
49. Cefalu, A., Abdel-Wahab, M., Peter, M., Wenzel, K., & Fritsch, D. (2013, July). Image based 3D Reconstruction in Cultural Heritage Preservation. In *ICINCO (1)* (pp. 201-205).
50. Wenzel, K., Rothermel, M., Fritsch, D., & Haala, N. (2013). Image acquisition and model selection for multi-view stereo. *Int. Arch. Photogramm. Remote Sens. Spatial Inf. Sci*, *40*(5W), 251-258.
51. Cavalagli, N., Gioffrè, M., Grassi, S., Gusella, V., Pepi, C., & Volpi, G. M. (2020). On the accuracy of UAV photogrammetric survey for the evaluation of historic masonry structural damages. *Procedia Structural Integrity*, *29*, 165-174.
52. Nayci, N. (2020). Architectural inventory and building condition assessment research on masonry structures of Kanlıdivane archaeological site, Mersin. *Cultural Heritage and Science*, *1*(1), 32-38.

Advanced UAV
http://publish.mersin.edu.tr/index.php/uav
e-ISSN 2822-6976

Evolution of the Main Crater, Irazú Volcano National Park, Costa Rica – Consumer Drones in professional research

Ian Godfrey*[1], José Pablo Sibaja Brenes [1], Maria Martínez Cruz [2], Khadija Meghraoui [3]

[1]Universidad Nacional, Laboratory of Atmospheric Chemistry Costa Rica, igodfrey@mail.usf.edu; Jose.sibaja.brenes@una.cr
[2]Universidad Nacional, Volcanological and Seismological Observatory of Costa Rica, Maria.martinez.cruz@una.cr
[3]Unit of Geospatial Technologies for Smart Decision. Hassan II Institute of Agronomy and Veterinary Medicine, Morocco, k.meghraoui@iav.ac.ma

Cite this study: Godfrey, I., Avard, G., Brenes, J. P. S., Cruz, M. M., & Meghraoui, K. (2022). Evolution of the Main Crater, Irazú Volcano National Park, Costa Rica – Consumer Drones in professional research. Advanced UAV, 2 (2), 65-85

Keywords
Unmanned Aerial System
Remote Control
Volcanic Environment
Irazú Volcano
Costa Rica

Research Article
Received: 05.10.2022
Revised: 10.11.2022
Accepted: 18.11.2022
Published: 30.11.2022

Abstract

There has been significant cracking and erosion on the south crater wall of the Main Crater below the area where tourists gather to view the main feature of the park; The Main Crater. By deploying the EVO Lite+ drone system we will be able to document any increase in erosion or cracking within the Main Crater, we will search for areas subject to future rock falls within the Main Crater, the UAS observation strategy will also be innovative as it offers a new and unique perspective of the volcano summit and interior structures of the Main Crater. By using the Lite+ system we will check for lake water levels, areas of mineralization or crystallization, and any potential vents degassing volcanic emissions, we will look for subaquatic fumaroles releasing gases via bubbles and try to film them for frequency and size documentation. The qualitative analysis of the Irazú Volcano Main Crater will show changes in morphology and illustrate how consumer drones can be used for professional research.

1. Introduction

Previous researchers use small single engine aircraft to observe volcanoes with thermal cameras visible only through a glass window in the bottom of the aircraft. Drones have since revolutionized this application as they can be flown so much closer to the volcanic caldera and can use specialized equipment such as thermal IR imaging cameras, LiDar 3-D mapping and gas detection equipment. Elevation of topography is very important UAS application in volcanic environments especially after eruptions to visualize geological changes and estimate the amount of ejected material after eruptions. UAS have played a significant role in helping geologists obtain this data.

The main field work objective was to launch the Autel Lite Drone into the Main Crater of the Irazú Volcano National Park in Costa Rica. We tried to document everything down to crater floor with detailed photos and video not obtainable from ground perspectives. Areas such as the crater lake. We wanted to observe water levels, any potential bubbles, rockslides, the Diego de la Haya crater and any potential cracking! We wanted to obtain videography of Diego de la Haya crater walls especially the cracking section and south crater wall. Over flights were planned from West to East passing all 5 craters, return flights designed to film the same thing gather videography from the aerial perspective.

Figure 1 & 2. Main Crater of the Irazú Volcano National Park 2020 & Autel Lite + (Red) Operational Flight Missions Plan for inside the Main Crater of the Irazú Volcano

2. Material and Method

2.1. UAS

The EVO Lite + drone by Autel Robotics has an air frame made of 3-D printed carbon fiber designed and built for superior strength. The drone has a total flight time of 40 minutes and weighs a total of 835 grams. This UAS has an 800-meter maximum flight altitude starting at the takeoff position and a 5000-meter maximum operational ceiling. The Autel EVO Lite + drone can withstand 32-38 mph wind gusts and has a level 7 wind resistance rating. The Autel EVO Lite + drones are also equipped with several wide-angle obstacle avoidance sensors. The airframe places these sensors facing forwards, downwards and in the rear facing backwards. These obstacle avoidance sensors will automatically detect tree branches and other potential obstacles and slow or stop the drone. Once obstacles are detected the Remote Controller will make an alarming sound to notify the pilot what is happening.

2.2. Camera

There are two camera sensors capable of collecting 20MP photo images and 6k /30fps video from the 1-inch CMOS sensor. This 20MP sensor uses larger pixels allowing for increased amounts of light and reduced interference. There is an F/2.8 – F/11 adjustable aperture, contrast focus, and is mounted to a 3-axis gimbal. This camera sensor was specifically designed for low light settings; the camera has 16x digital zoom. The low light videography capabilities are the result of the Moonlight Algorithm making the device ideal for documenting geographical aspects during the twilight hours of the day. The full view of the very wide active crater of the Irazú Volcano was photographed with the 1-inch CMOS sensor and can be seen from the UAS perspective in clear detail below.

Figure 3. Active Main Crater of the Irazú Volcano National Park Costa Rica September 2022


Figure 4 & 5. Autel Lite + Drone over the Main Crater of the Irazú Volcano National Park

2.3. Software Application

Autel Sky is the app associated with the Autel Lite + drone. This app features several advanced maneuvers preprogramed into the drone; Rocket, Orbit, Flick and Fade Away. The system also has a following option called Dynamic Tracker 2.1. This function makes the drone automatically follow the selected targeted subject selected by the remote pilot in command. Skylink insures stable long-range connection capable of transmitting video from over 7 miles away using the triple frequency system designed to reduce interference.

2.4. Flight Mission Planning

Several flight missions were planned for the Crater Sector of the Irazú Volcano National Park. By using Google Earth UAV pilots can check terrain and elevation differences for their planned drone flight path. By using this preflight strategy risks are reduced because remote pilots can check distances, altitudes, potential flight path obstructions and get a good idea of the topography of the area where flights are being planned.

Figure 6 & 7. Autel Lite + (Red) Operational Flight Missions Crater Sector of the Irazú Volcano

Figure 8 & 9. Autel Lite + (Red) Operational Flight Missions Altitude and Terrain Check Diego Crater Irazú Volcano

2.5. Evolution of the Irazú Volcano National Park

Costa Rica has a complex underlying tectonic framework. This is a direct result of the interaction between the Cocos, Caribbean, Nazca plates interacting along with the Panama block. The interaction between these four microplates creates the frequent earthquakes and volcanic activity in Costa Rica. The 2006 publication titled; "Recent volcanic history of Irazú volcano, Costa Rica: Alternation and mixing of two magma batches, and pervasive mixing," by Guillermo E. Alvarado resulted in several significant findings. Probably most importantly two distinct magma batches were identified. Methods such as seismological, magmatic and geological data were all combined for analysis which showed the presence of two small shallow magma chambers beneath the Main Crater at the Irazú volcano summit. Much of the northern volcano flank is not easily accessible and is completely covered be dense rain forests [1].

2.6. Using consumer drones in professional research

Using consumer drones in professional research was the main objective of this project and to show how they can be used for expanding scientific research. For the UAS flights the plan was to visit the Irazú Volcano National Park in Costa Rica with the Autel EVO Lite + UAS. The Irazú volcano last erupted in 1963 and continued eruptive behavior until 1965. At the Irazú volcano which is the highest volcano in Costa Rica, strong prevailing winds and gusts of various directions can create atmospheric conditions extremely complicated for remote pilots. The Autel Lite + drones were able to withstand 37 knots and were therefore strategically selected for this assignment.

In the national park system of Costa Rica special SINAC permitting is required to use drones on this land. "Estudio de las emisions volcanicas y su afectacion a la poblacion cercana." Permit # 112000166 for The Laboratory of Atmospheric Chemistry, Universidad Nacional LAQAT-UNA. The Autel EVO Lite + drones were used to document several aspects of the Main Crater of the Irazú volcano. Several features and detailed knowledge of these features collectively contribute to a greater understanding of the volcanic processes of these complex and dynamic systems.

Our UAS monitoring program began in January of 2020. We started using affordable consumer drones instead of enterprise drones in this research initiative due to the overall risk associated with flying UAS in volcanic environments. Images from our 2020 surveillance flights can be observed below. At the time of these flights there was a very light blue crater lake with a small island in the middle a bolder left from the 2019 rockfall and seiche.


Figures 10 & 11. Main Crater of the Irazú Volcano Main Crater January 2020


Figures 12 & 13. Main Crater of the Irazú Volcano National Park January 2020

The Autel EVO Lite + drone allowed us to get close detailed images and video from perspectives not obtainable from the main lookout observation point. In the past there were five open degassing vents on the crater floor only periodically visible when the crater lake was completely evaporated in (2013). We expected to observe this area and look for any potential bubbles with the detailed 6k video camera, but to our surprise on September 12th, 2022 on the day of our first visit, there was an extremely small lake more like a puddle and the crater lake was gone. The Cerro Alto Grande and the Río Toro Amarillo valley located in between the Irazú and Turrialba volcanoes was formed by erosion before the Diego de la Haya eruption activity. In the upper regions of the Diego de la Haya crater where observers can see the distinct difference in the two basaltic andesite lava flows. (1)

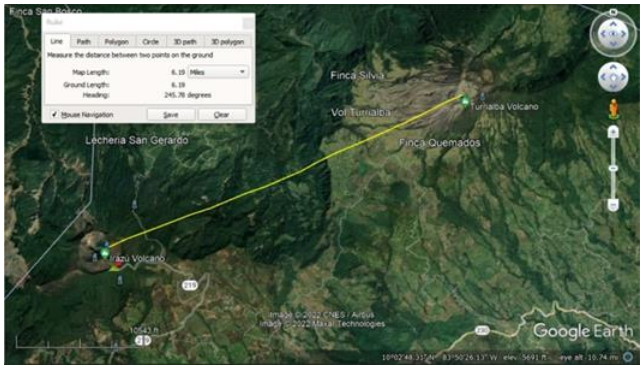

Figure 14 & 15. Google Earth Image - Distance Between Irazu and Turrialba

The volcanic front of Costa Rica lies parallel to the Mid Atlantic Trench and separates the Caribbean and Cocos tectonic plate. The volcanic front of Costa Rica and the Atirro-Río Sucio Fault directly intersects the Main Crater of the Irazú Volcano. In 1994 a partial collapse left a strange area below the Main Crater of the Irazú Volcano exposed, scientists found caves here and named them "Cueva de los Minerales" the newly discovered cave sectored allowed researchers an opportunity to better understand how the uplifting of volcanic gases combined with water seepage from the crater lake of the active Main Crater created hydrothermal interactions which created such a diverse collection of mineralogical deposits. This area has obvious hydrothermalism and significant CO_2 degassing from passive fumaroles located inside the caves [2].

3. Results

3.1. Main Crater Irazú Volcano, Crater Lake

In the research paper titled; "Extremely High Diversity of Sulfate Minerals in Caves of the Irazu Volcano (Costa Rica) Related to Crater Lake and Fumarolic Activity, by Andres Ulloa; The publication explains that since the eruptive activity seen from 1962-1965 there has been an intermittent volcanic lake inside of the active Main Crater of the Irazú Volcano. The lake remained in the crater from 1965 until 2013 when it evaporated and disappeared due to water seepage. The lake began the reformation process in 2017, studies showed that the temperature of the lake water fluctuated between 16-35°C and the water's pH also fluctuated as much as 3.0-5.85. One of the most obvious geomorphic fluctuations that consistently captures interest is the crater lake water color. Scientists have documented the water color of the Irazú volcano crater lake as red, blue, green, turquoise, and yellow water colors. [2].

Figure 16 & 17. Irazú Main Crater January 2020

The crater floor is a porous rocky and sandy environment, and due to the permeability on the crater floor large amounts of draining occur which contribute to the hydrothermal process creating the Cueva de los Minerales. This draining and periodic refilling due to rain fall in the region is a contributor to the frequently observed color fluctuations of the crater lake. The report explained that there were fumaroles documented on the floor of the Main Crater from 1998-2001, and that there is most likely a hydrothermal connection between the Main Crater of the Irazú Volcano and the Río Cucio volcanic hot springs on the northern flank of the Irazú volcano. (2)

Figure 18 & 19. Irazú Main Crater October 2017

Figure 20 & 21. Irazú Main Crater Febuary 2019

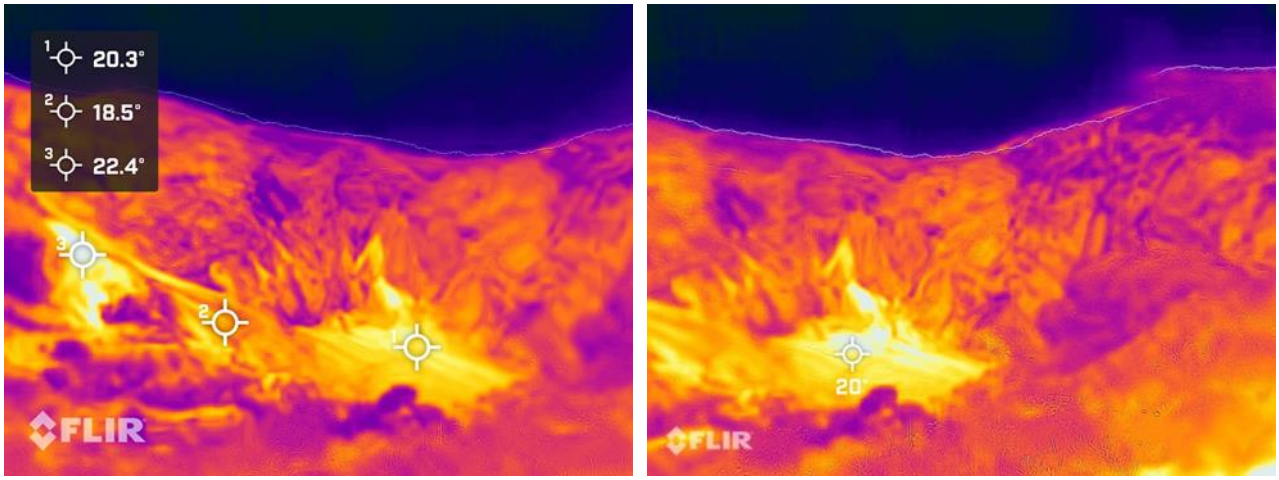

Figure 22 & 23. Thermal Images in Degrees Fahrenheit of the Irazú Volcano Main Crater

The thermal images of the Main Crater show no crater lake; therefore, we were able to take thermal images of the crater floor. The crater lake located inside the main crater of the Irazú volcano is part of a sophisticated hydrothermal system of the volcano which discharges liquids through several springs on the northern flank of Irazú. The spring is an example of how the hydrothermal system of the Irazú volcano interconnects various geophysical aspects of the Irazú Volcano. The hydrothermal system of the Irazú Volcano has various aspects like the crater lake, spring and fumarole which are all connected by the hydrothermal system of the volcano.

Figure 24 & 25. Río Sucio Río Caliente Volcanic Hot Spring of Irazú Volcano Analysis April 2022

Several aspects of the volcanic crater lake can offer insight into the level of degassing seen coming from the Main Crater of the Irazú Volcano, such as water levels and water color for example. The camera on the Autel Lite + was specifically selected to document the exact color of the crater lake water. The crater lake water color was a combination of interacting processes. For example, 1. colloidal particles, volcanic minerals defracting light, 2. algae a single celled nucleus-bearing aquatic photosynthetic organism, 3. gas bubbles and dissolved emissions in the water also contribute to the water color. Upon launching the UAS in September of 2022, there was no lake remaining.

Previous work on the Main Crater of the Irazú Volcano showed that gas anololies existed both within the Main Crater and on the northern flank of the Irazú Volcano. The has been degassing documented coming from the northern flank of the Irazú Volcano. This area where the caves are located is extremely steep and very difficult to acess, and therefore monitoring this region with a UAS becomes a prized application for the surveillance of the Irazú Volcano National Park [3].

Since 1994 the SINAC and OVSCORI-UNA have been watching Irazú closley, using UAS to periodically take images for 3-D Digitan Surface Models which you can watch on Youtube via the link below. After the disappearance of the crater lake in 2013 research of the Main Crater showed no increase of volcanic activity and studies concludes the disappearance was likely due to seepage rather than evaporation [3].

Figure 26 & 27. Floor of the Main Crater Irazú Volcano National Park September 2022

All of these aspects contribute to the water color of the crater lake. In addition, due to periodic eruptions and the continuous release of SO2 coming from the Turrialba volcano just 6.2 miles to the east of the Irazú volcano Main Crater, acidic rain periodically dispersed around the Irazú volcano. 4. Acid rain adds another variable which contributes to the color of the crater lake located inside the Main Crater of the Irazú volcano.

Enhanced oxidative conditions are a significant factor in this region due to the consistent release of volcanic emissions seen coming from the Turrialba volcano. There are several contributing factors that all play a part and have an effect on the water color of the majestic crater lake inside the active crater of the Irazú volcano.

For the first time since 2013 the Main Crater of the Irazú Volcano no longer has a crater lake. By deploying the Autel EVO Lite + drone we were able to use an affordable consumer drone for professional volcanic surveillance of an active crater. Several aspects were documented to precise detail using the zoom and high resolution 6k camera for videography. All rock falls were documented from the aerial perspective, along with the crater floor, plant vegetation inside the crater, cracking and the existence of potential waterfalls, were all recorded in high resolution and photographed for Volcanic and Seismic Observatory of Costa Rica OVSCORI-UNA and the Laboratory of Atmospheric Chemistry LAQAT-UNA Universidad Nacional.


Figure 27 & 28. Floor of the Main Crater Irazú Volcano National Park September 2022


Figure 28 & 29. Floor of the Main Crater Irazú Volcano National Park September 2022

3.2. Main Crater - Rock falls


Figure 30 & 31 - Rockfall formation left from the 2019 material release and resulting sieche September 2022

Inside the Main Crater there are three areas of significant rock fall which geologists and SINAC park rangers are consistently observing and monitoring. In May of 2019 heavy rain in the region and increased seismic activity deriving from the fault line located directly below the Main Crater of the Irazu Volcano both contributed to a massive rock fall on the west side of the Main Crater which fell off and created a seiche or a wave inside an enclosed body of water, and then deposited a significant amount of material into the lake which drastically changed the color of the crater lake.

In the publication; Study of Turquoise and Bright Sky Blue Appearing Freshwater Bodies for the International Journal of Geology, Earth & Enviromental Sciences the paper explains - “Suspended and dissolved particles influence the color of water. Turquoise and bright sky-blue appearing fresh water bodies are found in different parts of the world in different sets of environmental conditions. Glacial-fed lakes also appear turquoise, crater lakes also bear turquoise color and calcium carbonate rich water bodies also appear turquoise.” [4].

The exotic light blue vibrant color of the crater lake located in the Main Crater of the Irazú Volcano is mainly due to the scattering of light in the blue and green wavelengths due to the presence of colloidal particles deriving

from the volcanic sediment and rocks the rainwater interacts with before collecting in the summit crates of the Irazú Volcano National Park in Costa Rica. These particles become suspended in the crater lakes and can collect at the water's surface refracting the light in the blue and green wavelength particularly at the deepest part of the lake where more suspended particles can accumulate. Other factors do play a role in the color seen by observers such as temperature, pH levels, EC or electrical conductivity, total dissolved solids in the water body, density and the amount of total dissolved oxygen or O_2. pH fluctuations have been shown to have direct color changing results as the changes in pH induces the growth of these particles from 184nm to 566nm and therefore the light scattering occurs mostly in the blue region of the visible spectrum [4].


Figure 32 & 33. Irazú Volcano May 2019 after the seiche inside the Main Crater

Previously researchers conducting field work for the Volcanic and Seismic Observatory of Costa Rica OVSCORI-UNA and the Laboratory of Atmospheric Chemistry LAQAT-UNA Universidad Nacional documented the waterfall Río Celeste of the Tenorio Volcano complex and found that during the investigation researchers on a global scale found blue-green and exotic turquoise water bodies with correlation to active volcanic regions. Volcanic crater lakes with a wide variety of color exist in countries like Iceland, Japan and New Zealand all of which have active volcanoes. It was found that the crater lake water had aqueous colloidal silica particles which contributed to the light scattering of the natural sunlight. Both Rayleight scattering and Mie scattering of sunlight can occur from the presence of these aqueous colloidal silica particles. For example, the Yugama Crater Lake of Mount Shirane in Japan was studied and the analysis showed that the crater lake water color was a result of the water chemistry which was responsible for both Mie and Raylight scattering by colloidal sulfur particles. (5)


Figure 34 & 35. Main Crater of Irazú Volcano January 2020


Figure 36 & 37. Main Crater of Irazú Volcano January 2020


Figure 38 & 39. Main Crater of Irazú Volcano January 2020


Figure 40 & 41. Rockfall from the North Eastern edge of the crater rim September 2022


Figure 42 & 43. Rock Fall Area West End of Main Crater UAS Perspective September 2022


Figure 44 & 45. Rock Fall Area West End of Main Crater UAS Perspective September 2022

There are three areas of rock falls being monitored today which are located on the west, north-east and south-east of the main crater. By using the drone from the very center of the crater we were able to get a 360° view of not only the crater but the details of each individual rock fall as well. The results of these UAS flights will probable gain appreciation when the lake water begins to refill and it is no longer possible to view the crater floor.

The fault line intersecting the Main Crater of the Irazu volcano which is part of the volcanic front of Costa Rica is the Atirro-Río Sucio Fault that directly intersects the Main Crater of the Irazú Volcano. Any kind of seismic activity in the area can influence the rock falls inside the Main Crater. Heavy Thunderstorms passing by and increased rain fall will also contribute to the rock falls and any potential land slide within the Main Crater of the Irazú Volcano.

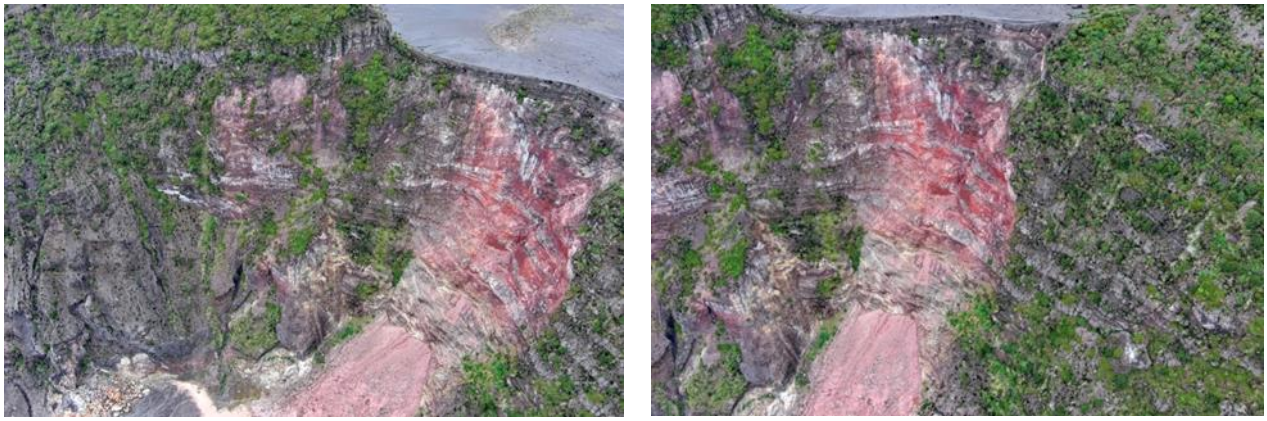

Figure 46& 47. Rock Fall Area East End of Main Crater UAS Perspective September 2022

Figure 48 & 49. Rock Fall Area West End of Main Crater UAS Perspective September 2022

3.3. Main Crater - Vegetation on Interior Crater Walls

Usually, plants growing naturally inside of an active volcanic crater are exposed to above average levels of CO_2. Active volcanoes continuously release CO_2, yet the rate of the degassing will fluctuate. The ecosystems of volcanic climates are both valuable and fragile. High altitude summit areas in Central America are particularly interesting like the Irazú Volcano National Park in Costa Rica. The Irazú Volcano National Park consists of once active Main Crater and a degassing cave named “Cueva de los Minerales” and fumarole and volcanic hot spring named “Río Caliente” on the northern flake of the volcano. All of these areas are exposed to elevated levels of atmospheric CO_2. Tropical forests represent around 40% of terrestrial net primary production worldwide; they store 25% of biomass carbon, and may possibly contain 50% of all species on Earth. Still, the forecasted future effects from increasing levels of atmospheric CO_2 on a global scale relative to tropical plants response is not yet fully understood. There are over 200 active volcanic systems located in the tropics many of which are covered in thick vegetation [6].

The diverse high altitude tropical vegetation located inside the Main Crater of the Irazu volcano holds much of the soil together with tough root systems. Possibly due to the acid rain deriving from the increased activity and degassing of the Turrialba volcano 6.5 miles east of the Irazu volcano many of these plant species have burn marks on their foliage. Naturally this acidic rain would have had a severe effect on the root system as well. Acid rain therefore contributes to erosion. This may have been a significant factor contributing to the 2019 rockfall. Monitoring vegetation inside the Main Crater is an important observational aspect of monitoring the Main Crater of the Irazu volcano.


Figure 50 & 51. Vegetation on South End of Main Crater Wall September 2022


Figure 52 & 53. Vegetation on South End and East End of Main Crater Wall September 2022

Burnt vegetation found inside the Irazu Volcano National Park from 2017 through 2020 had mostly vanished underneath the thick vegetation from healthy regrowth. This burnt vegetation was due to acidic rain deriving from the SO_2 being released from the Turrialba Volcano.

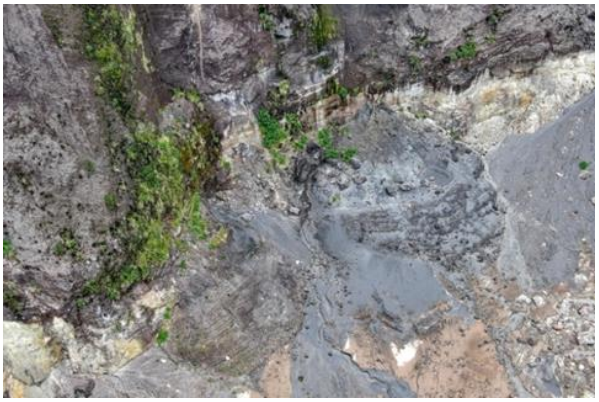


Figure 54 & 55. Floor of the Main Crater Irazú Volcano National Park September 2022


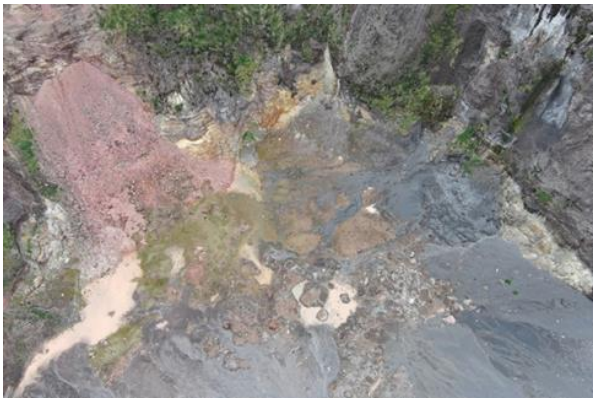

Figure 56 & 57. Floor of the Main Crater Irazú Volcano National Park September 2022

3.4. Main Crater - Cracking

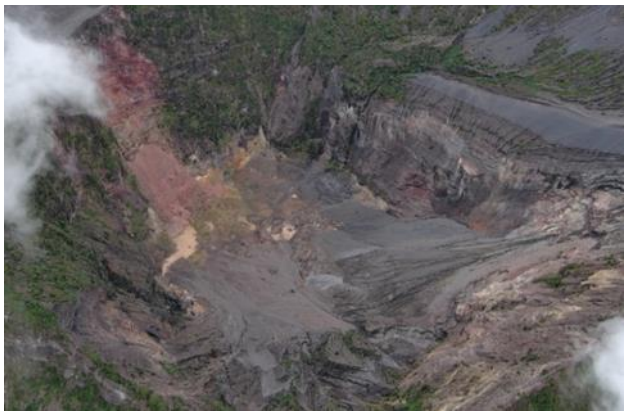


Figure 58 & 59. Main Crater UAS Perspective September 2022

Using consumer drones in January of 2020 starting on the northern rim of the Main Crater we observed cracking in the area that separates the Main Crater from the Diego de la Haya crater. The Diego de la Haya crater is another prehistorical crater located inside the Irazu Volcano National Park which last erupted in 1723. By using Autel EVO Lite + UAS which is an affordable consumer drone we monitored these cracks which are not visible from the perspective from the main lookout point. On September 12th, 2022 we monitored the area where these cracks were found to see if they widened, increased in number or had shown any signs of significant geological change. These cracks were located just below the crater rim on the upper south-eastern section of the Main Crater. Since many park visitors and observers walk around the Playa Hermosa, monitoring these cracks with consumer drones has become a valued UAS application which contributes to the safety of people visiting the national park.


Figure 60 & 61. Cracking in Main Crater January of 2020


Figure 62 & 63. Area of Cracking Documented with the Autel Evo Lite + drone September 12th, 2022

3.5. Main Crater - Waterfall

Consumer drones can contribute to a better understanding of the volcanic hydrothermal system, Periodically there has been a waterfall observed coming from below the Playa Hermosa crater (observational area) in the Irazu Volcano National Park. This waterfall was located on the southern end of the Main Crater and can only be seen from a few exclusive trails located on the northern rim of the Main Crater which are not accessible by the general public. The Autel Lite + consumer drone allowed us to check if this waterfall still existed and observe the potential water flow levels.


Figure 64 & 65. Waterfall Area South Rim of Main Crater September 2022

3.6. Diego de la Haya


Figure 66 & 67. Diego de la Haya Prehistorical Volcanic Crater September 2022

All together there are five craters within the area of the Irazú Volcano National Park. The Diego de la Haya crater is to the east of the active Main Crater and last erupted in 1723 when Diego de la Haya was the Spanish governor of the Cartigo Province in Costa Rica. This was a severe eruption that had a drastic effect on the communities of Cartago. Today the topography of the Irazú Volcano National Park including the Diego de la Haya crater is a complex and beautiful landscape, one that can create issues for remote pilots. Around the Diego de la Haya crater large crater walls can creat interfierance and contribute to drones disconnecting. This never happened with the Evo Lite + UAS during our flight missions but can happen and is something remote pilots should be aware of when operating in areas of complex topography. Sensors on the Evo Lite + drone prevented the UAS from accadently colliding with crater walls and other obsticles presented in the complexed topography such as trees, radio antenas, and crater walls.

The Evo Lite plus drone performed exceptionally well in the volcanic environment. Wind gusts were no issue and the drone operated perfectly at these high altitudes with reduced atmospheric density. The Evo Lite + drone were flown for a continuous period of about 2.5 hours at the Irazú Volcano National Park. Each flight mission was dedicated towards a different aspect of the Main Crater of the Irazú Volcano. Batteries were immediately switched and flights continued without any delay. In between each flight, while changing the batteries, the rotary systems on all four arms were checked for heat! Any kind of temperature increase on the rotary system from high use may mean a cooldown period is needed for the drone. At no point did the Lite + drone require any sort of cooldown person and we were able to quickly switch the batteries and move forward with the next flight mission. At no time was there any disconnect between the drone itself and the remote control. Special attention was given to the RC drone connectivity bar graph in the upper right on the control screen and there was very little connection

reduction despite the drone being sent far away for volcanic flight missions covering great distances in difficult conditions. Atmospheric humidity and Zero Visibility occurred several times as cloud coverage can move rapidly at these altitudes. Considering the drone was flown in high altitude volcanic terrain in the Central American Tropics, the device was durable in transit and during periods of climbing, it was easy to unfold and deploy without waiting for any kind of warm up period, we were able to launch and land directly from our hands which was helpful as there are uneven rocky terrain around the Irazú volcano which is not ideal for launching and landing from the ground.

3.7. Topography of Irazú Volcano National Park

Figure 68 & 69. Western Main Crater Rim of the Irazú Volcano September 2022

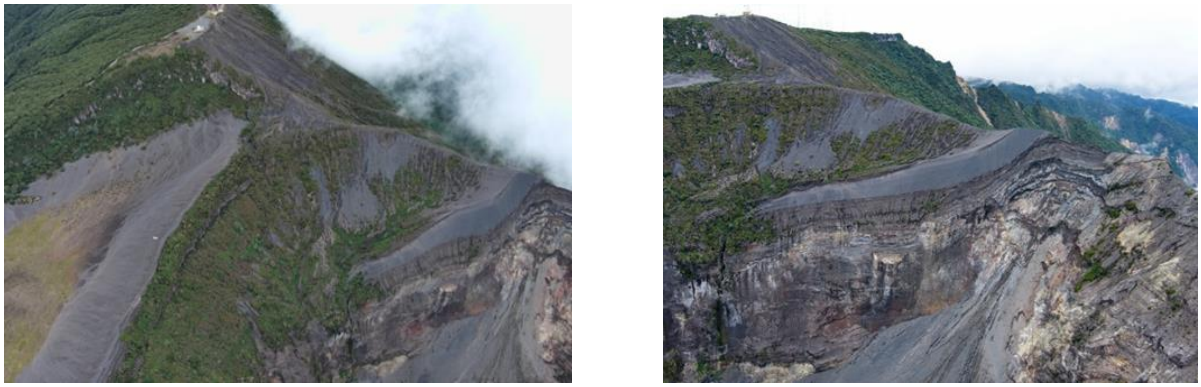

Figure 70 & 71. Irazú Volcano National Park September 2022

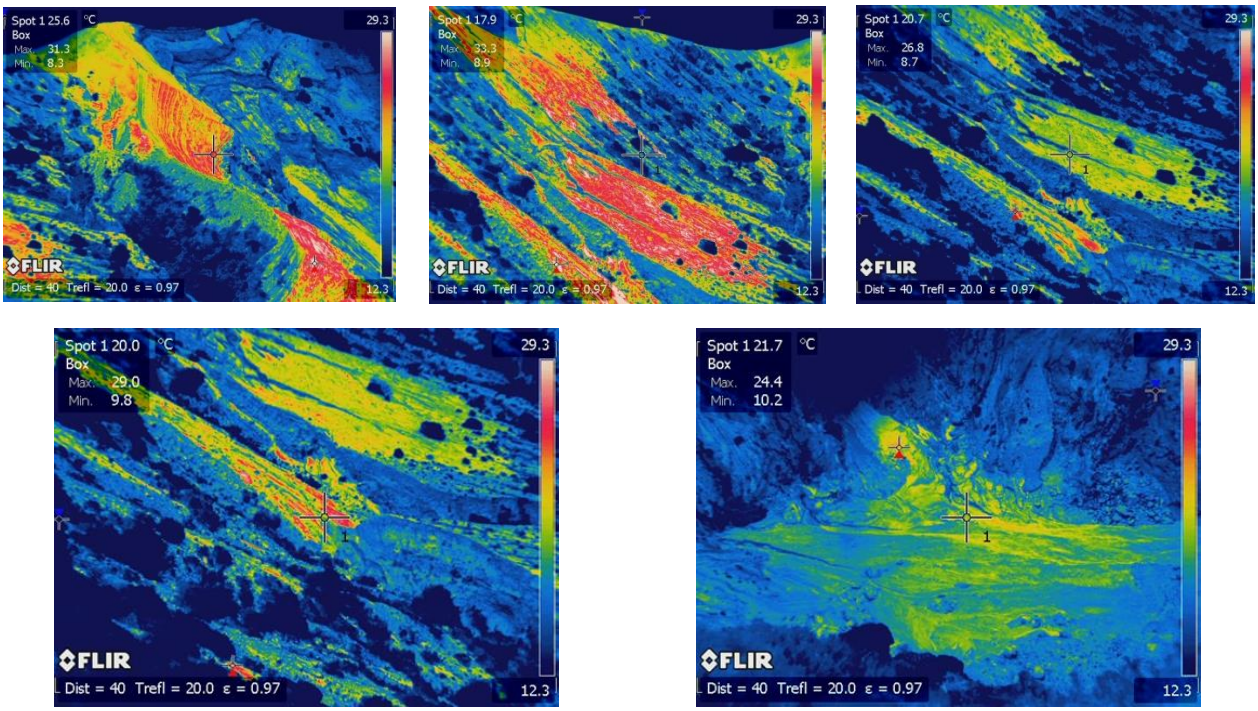

Figure 72 – 76 - FLIR Images from Maria Martínez Cruz

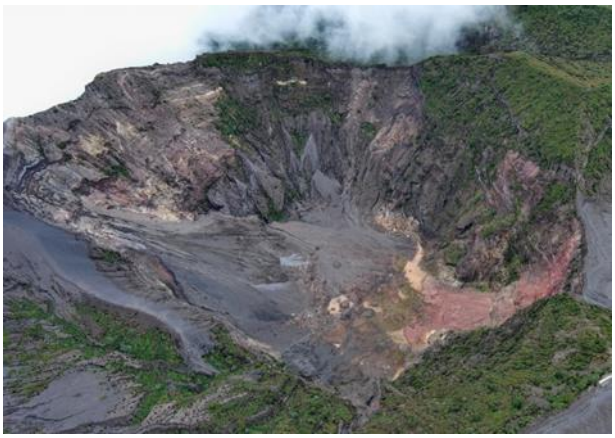


Figure 77 & 78. Aerial View of the Main Crater of the Irazú Volcano National Park September 2022

Changes in gas composition and emission rate are likely one of the first signs of unrest at volcanoes. By expanding our gas detection capabilities and broadening our UAS application to include volcanic emission tracking, we can begin monitoring more emissions from a larger number of volcanoes and through increased frequency and reliability along with using previously confirmed early warning detection systems and data analysis significant improvements can be made to our strategy and ability to predict volcanic eruptions. Carbon dioxide CO_2 can be from both magmatic sources and hydrothermal as well; this gas can travel along fault lines; it can be periodically released from cracks and fractures in the volcanic edifice and it can also diffuse through soils surrounding the active crater. CO_2 can also be released from soils that are distant from the active crater and fumarolic field making gas measurements important for surveying and tracking emissions in other volcanic areas further away from the areas of visible activity [7].

It's possible for phreatic and hydrothermal eruptions to occur in hydrothermal systems where vents are located such as the Main Crater of the Irazú Volcano National Park. Sealing can be small or large and generalized or localized situations have both been documented. When lakes occupy active volcanic craters they can trap gases and accumulate high temperatures [8].

Using UAS can help researcher study active crater morphology and geological changes. These UAS can carry scientific equipment to document volcanic gas emissions, take thermal images and collect water samples. UAS can also be used to monitor and document ozone depletion following future volcanic eruptions [9]. UAS can also greatly assist via aerial survey of volcanic regions covered in thick tropical vegetation. Still no phreatic nor hydrothermal eruption has been accurately predicted, yet the UAS can be a tool volcanologists can use to gather additional information not obtainable from ground level observations. The UAS can also be used to enter the danger zone such as active craters and gather additional data on the area of interest for the scientific community.

Figure 79. Layering of East Side of Main Crater Wall of the Irazú Volcano September 2022

4. Discussion

Piloting remote aircraft in high altitude volcanic environments is one of the most complex and risky situations for a drone pilot. Is the data more valuable than the drone? Is a frequent question remote pilots often ask themselves before the flight and at the point in the flight where the drone begins collecting great data, prized photos and excellent video, but riskier conditions start settling in. For example, of a complex flight for a remote pilot operating in a volcanic environment is when it's clear where the drone around 600 meters away from the home point and it starts raining at the remote pilot's location. These situations must be planned for to the best if the remote pilot in command capabilities.

Unaccounted for situations will still arise, but with proper training and knowledge of these environments obtaining the data points from the planned flights is certainly possible. When planning to operate drones in volcanic environments it's essential to check the weather forecasts for the days you're planning the mission and to consistently monitor any potential changes on Windy.

Climatic stability in volcanic regions can change in less than one minute. And with that comes relative humidity fluctuations, 80% change in visibility conditions, wind speed change, wind direction change, enhancing wind gusts. Therefore, extreme presentation is necessary for the remote pilot to obtain as much geological and atmospheric knowledge of the region before flights. In Costa Rica while studying the Irazú volcano at 3,432 meters in altitude the poor visibility and cloud coverage changes were frequently avoided with the assistance of a visual observer and the decision to increase or decrease altitude to avoid the passing clouds. Obviously, these decisions are made by the remote pilot in command who must also consider the altitude of the flight and the terrain formations directly below the drone.

Probably one of the most impressive drone surveys of a volcano was conducted in 2016 and 2017; Researchers from Universidad Nacional collaborated on an international undertaking where advanced remote pilots flew drones at both the Turrialba Volcano in Costa Rica and the Masaya Volcano in Nicaragua. The flight mission objectives were to measure the degassing deriving from the active craters. At the time these two volcanoes were the largest time integrated source of CO_2 in all of Central America. During the 2016-2017 period when the research project was conducted both volcanic systems were actively degassing and showing increased signs of a potential eruption. Researchers and remote pilots managing this project noted that; Remote pilots operating in high altitude volcanic environments especially active systems had to be particularly concerned with the hardware because the devices are often subject to harsh field conditions. These researchers developed a fly/no fly checklist which has served to be very useful to many remote pilots learning to operate UAS in these climatic conditions. Several points were included into the checklist such as wind, and wind gusts, unexpected turbulence, weather, steep relief, summit risks, convicting volcanic gases, obstacles in flight path, eruption columns, battery limitations, communication limitations, communication issues from close by radio towers, static electricity from volcanic ash, and any potential line of sight complications between the remote pilot and the drone itself. (10)

4.1. Flight Risk/Reward Ratio

The Risk/Reward ratio for flying a drone consists of weighing the value of the drone itself (not including the Remote Controlo batteries in the case) against the value of the data which can be obtained during that particular flight. Is the data being gathered and stored more important than the drone itself? The answer is usually no, yet certain circumstances like an eruption for example, may tip the scale of the UAS Risk/Reward ratio in favor of conducting the risky flight mission. In these circumstances it's recommended to use the most economically priced UAS available in case the drone is lost forever.

4.2. Extra Micro SD cards

It's recommended that remote pilots flying drones in volcanic regions carry extra Micro SD cards in their drone case because valuable data may be obtained and the pilot may want to continue with more flight missions. By changing the Micro SD card, the data from the previous flight is guaranteed to be returning to the lab for processing. Sometimes valuable photos used to generate 3-D Digital Surface Model have been collected and the remaining flight missions are non-essential, in these situations it's important that the remote pilot remember to switch the Micro SD cards in-between flights. It's usually possible to specifically set the drone to save onto the mobile device being used with the RC to operate the drone this can also greatly serve remote pilots operating in complex climates.

4.3. Reduction in Altitude

When flying in volcanic craters there is not just the altitude in meters Above Ground Level or AGL like in the Part 107 remote pilot listening test. When piloting remote aircraft in volcanic terrain one must also consider the atmosphere below, just as importantly if not more significant is the reduction in altitude (Below Ground Level) BGL. A critical point of preflight planning as flying into an active crater is not already complicated enough but

one must consider the Return to Home RTH flight will most likely require more battery energy than the flight path used to enter the volcanic crater because the drone needs to lift itself higher to get out of the crater. The same concept applies when launching from a volcanic summit and surveying the flanks or slopes of a volcano; the drone flight altitude will be lower than the altitude of the home point.

4.4. Climatic Conditions

In these high-altitude volcanoes in Costa Rica random periodic rain showers pass by sometimes quite quickly perhaps 10 minutes from start to finish for example. Remote pilots will need to wait for their next window of opportunity and then weight the flight risk/reward ratio. These frequent rain showers can last from 10 minutes to over a full day.

4.5. Launching and Landing

Successful takeoff and return to home with the drone can also be a bit more complicated here as well since the launch and land terrain is often inclined rocky and grassy areas that are usually unstable. Using legs to extend the drone towards the ground are highly recommended. Remote piloting in these volcanic climates is usually assisted by the aircrafts ability to launch and land from the palm of the hand.

4.6. Clouds

Rapidly passing small clouds will have a direct effect on the drone's connection to the GPS satellites. They are directly responsible for the 80% fluctuation in visibility, and Relative Humidity RH.

4.7. Risks

Degassing fumaroles, steep slopes, and unconventional hidden factors all play a role in the environment a volcanic remote pilot must operate in. There can be visibility complication due to water vapor and volcanic degassing. Visibility issues can impact the drone itself and the display on the RC, and they can directly impact the remote pilot at the home point. For example, if a cloud passes and visibility is reduced by 70% at the home point than observing the drone via line of sight will be severely impacted. Tropical sunlight reflecting off the RC screen can all be challenging in volcanic environments so hat and sunglasses are quite essential. Usually there are people visiting or others studying these volcanoes and therefore it's highly recommended never to fly directly over any people, vehicles or valuable infrastructure such as National Park housing or equipment and especially telecommunications towers. Telecommunications towers are frequently located at volcanic peaks due to their strategically high location being ideal for broadcasting networks. These broadcast towers also contribute to interference between the drone and the RC. Flying with an insurance policy is always important for risk reduction.

4.8. Unforeseen variables

Many unforeseen variables exist in these high-altitude volcanic regions. Birds, small single engine aircraft, and other wild animals at ground level can be a distraction. Hardware malfunction is always possible and the remote pilot should take this into consideration before operating the UAS. Potentially distracting animals and degassing fumaroles at home point location all have an effect on the ability of the remote pilot to safety operate the drone, but also to collect the data and to return the drone back to the home point safely. Tourists and other people may approach and it important that the remote pilot be accompanied by a visual observe who is ready to stop the people from asking distracting questions and creating interruptions in areas with people around.

4.9. Altitude

One of the most complex remote flight climate conditions on Earth. The altitude above 10,000 feet has a different atmospheric make up with less 02 the air is thinner and operation of a remote aircraft becomes more complicated. Certain UAS have altitude ceilings which have significant improved over the past several years. For example, the max altitude of the Autel Lite + drone due to a reduction in air density in high altitudes flying a drone above 3,000 meters is significantly more complicated. How the drone hovers and uses batters is different, flight inclination is different and therefore the remote pilot must operate the UAS differently as well.

Temperature in these volcanic regions is significantly reduced relative to the tropical lowlands of Costa Rica, and therefore remote pilots must also consider the temperature of the air during the drone flight and how that will affect the equipment.

Between the lower air density due to altitude and reduced temperatures actual flight time will be reduced and this must be taken into consideration. Research with UAS pilots has shown pilots can expect a 10% reduction in battery preference every 2,000 meters. Remote flight operations will become extremely complicated at 4,000 meters and above, most drones will require proper modifications and specialized parts for these altitudes. There is greater wind turbulence inside craters, next to cliff faces and in valleys.

4.10. Lightning and thunderstorms

If there is a Thunderstorm it's an almost certainly to cancel the flight mission and postpone for a better day. If there are lightning strikes it's an outright stand down. Lighting will destroy the connection capabilities of the RC and drone and will cause a complete disconnect.


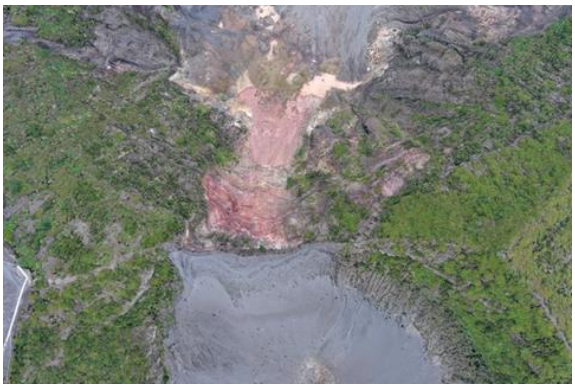

Figure 80 & 81. Irazú Volcano National Park September 2022

5. Conclusion

From the ground level there are significant restrictions for observing complex and dynamic volcanic systems. This limited perspective is enhanced exponentially by launching consumer drones. This increased the observational capabilities of researchers studying the Irazu volcano in 2022, the Autel EVO Lite + drone gave researchers studying the active Main Crater of the Irazu volcano a new enhanced perspective and greatly contributed to the gathering of valuable information associated with the Main Crater of the Irazu Volcano National Park in Costa Rica.


Figure 82 & 83. Main Crater Floor Irazú Volcano September 2022


Figure 84 & 85. Aerial View of the Entire Main Crater of the Irazú Volcano September 2022

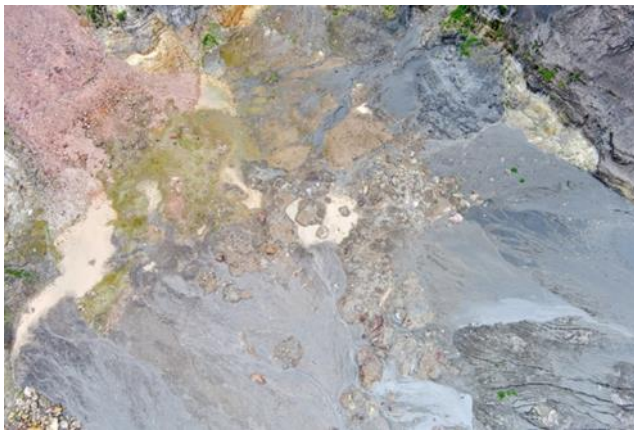


Figure 86 & 87. Aerial View of the Main Crater floor of the Irazú Volcano September 2022

The use of aerial photogrammetry assisted by drone in the field of morphological monitoring of volcanoes is an emerging technology that allows geoscientists to acquire more accurate spatial information.

The exploitation of derivative products, in particular orthophotos and digital models describing the forms of the land and the changes, makes it possible to have and identify the different features that may appear in these natural forms.

Differences and changes in topography can thus be determined using the volume differences between two separate states conducted a study based on aerial photogrammetry more particularly using UAV data to investigate the various changes of Mount Agung in Indonesia during the highest volcanic activity [11-12].

Researchers investigated the use of high-resolution UAV data for the generation of three-dimensional point clouds for the monitoring of the Stromboli volcano and emphasized the advantages of aerial photogrammetry for the geomorphological monitoring of these natural areas [13].

Figure 88. Aerial View of the Entire Main Crater of the Irazú Volcano September 2022

Acknowledgement

Ian Godfrey is a passionate explorer of the natural world, a writer, a Part 107 Remote Pilot and Thesis Advisor to the Laboratory of Atmospheric Chemistry Universidad Nacional Costa Rica. He has flown UAS into several high altitude active volcanic craters and a variety of industrial sites.

Funding

This research received no external funding.

Author contributions

Ian Godfrey: Conceptualization, Methodology, Software **José Pablo Sibaja Brenes:** Data curation, Writing-Original draft preparation, Software, Validation. **Maria Martínez Cruz:** Visualization, Investigation, **Khadija Meghraoui:** Writing-Reviewing and Editing.

Conflicts of interest

The authors declare no conflicts of interest.

References

1. Alvarado, G. E., Carr, M. J., Turrin, B. D., Swisher, C. C., Schmincke, H., & Hudnut, K. W. (2006). Recent volcanic history of Irazú volcano, Costa Rica: Alternation and mixing of two magma batches, and pervasive mixing. *SPECIAL PAPERS-GEOLOGICAL SOCIETY OF AMERICA*, *412*, 259.
2. Ulloa, A., Gázquez, F., Sanz-Arranz, A., Medina, J., Rull, F., Calaforra, J. M., ... & De Waele, J. (2018). Extremely high diversity of sulfate minerals in caves of the Irazú Volcano (Costa Rica) related to crater lake and fumarolic activity.
3. Epiard, M., Avard, G., De Moor, J. M., Martinez Cruz, M., Barrantes Castillo, G., & Bakkar, H. (2017). Relationship between diffuse CO2 degassing and volcanic activity. Case study of the Poás, Irazú, and Turrialba Volcanoes, Costa Rica. *Frontiers in Earth Science*, *5*, 71.
4. Kumar, V. (2016). Study on turquoise and bright sky-blue appearing freshwater bodies. *International Journal of Geology, Earth and Environmental Science*, *6*(1), 119-128.
5. Castellón, E., Martínez, M., Madrigal-Carballo, S., Arias, M. L., Vargas, W. E., & Chavarría, M. (2013). Scattering of light by colloidal aluminosilicate particles produces the unusual sky-blue color of Río Celeste (Tenorio volcano complex, Costa Rica). *Plos one*, *8*(9), e75165.
6. Bogue, R. R., Schwandner, F. M., Fisher, J. B., Pavlick, R., Magney, T. S., Famiglietti, C. A., ... & Duarte, E. (2019). Plant responses to volcanically elevated CO 2 in two Costa Rican forests. *Biogeosciences*, *16*(6), 1343-1360.
7. Kern, C., Aiuppa, A., & de Moor, J. M. (2022). A golden era for volcanic gas geochemistry?. *Bulletin of Volcanology*, *84*(5), 1-11.
8. Montanaro, C., Mick, E., Salas-Navarro, J., Caudron, C., Cronin, S. J., de Moor, J. M., ... & Strehlow, K. (2022). Phreatic and Hydrothermal Eruptions: From Overlooked to Looking Over. *Bulletin of Volcanology*, *84*(6), 1-16.
9. Eric Klobas, J., Wilmouth, D. M., Weisenstein, D. K., Anderson, J. G., & Salawitch, R. J. (2017). Ozone depletion following future volcanic eruptions. *Geophysical Research Letters*, *44*(14), 7490-7499.
10. Stix, J., de Moor, J. M., Rüdiger, J., Alan, A., Corrales, E., D'Arcy, F., ... & Liotta, M. (2018). Using drones and miniaturized instrumentation to study degassing at Turrialba and Masaya volcanoes, Central America. *Journal of Geophysical Research: Solid Earth*, *123*(8), 6501-6520.
11. Fedele, A., Somma, R., Troise, C., Holmberg, K., De Natale, G., & Matano, F. (2020). Time-lapse landform monitoring in the Pisciarelli (Campi Flegrei-Italy) fumarole field using UAV photogrammetry. *Remote Sensing*, *13*(1), 118.
12. Andaru, R., & Rau, J. Y. (2019). LAVA DOME CHANGES DETECTION AT AGUNG MOUNTAIN DURING HIGH LEVEL OF VOLCANIC ACTIVITY USING UAV PHOTOGRAMMETRY. *International Archives of the Photogrammetry, Remote Sensing & Spatial Information Sciences*, 173-179.
13. Gracchi, T., Tacconi Stefanelli, C., Rossi, G., Di Traglia, F., Nolesini, T., Tanteri, L., & Casagli, N. (2022). UAV-Based Multitemporal Remote Sensing Surveys of Volcano Unstable Flanks: A Case Study from Stromboli. *Remote Sensing*, *14*(10), 2489.

Advanced UAV
http://publish.mersin.edu.tr/index.php/uav
e-ISSN 2822-6976

Using UAS with Sniffer4D payload to document volcanic gas emissions for volcanic surveillance

Ian Godfrey [*1], José Pablo Sibaja Brenes [1], Maria Martínez Cruz [2], Khadija Meghraoui [3]

[1]Universidad Nacional, Laboratory of Atmospheric Chemistry Costa Rica, igodfrey@mail.usf.edu; Jose.sibaja.brenes@una.cr
[2]Universidad Nacional, Volcanological and Seismological Observatory of Costa Rica, Maria.martinez.cruz@una.cr
[3]Unit of Geospatial Technologies for Smart Decision. Hassan II Institute of Agronomy and Veterinary Medicine, Morocco, k.meghraoui@iav.ac.ma

Cite this study: Godfrey, I., Brenes, J. P. S., Cruz, M. M., & Meghraoui, K. (2022). Using UAS with Sniffer4D payload to document volcanic gas emissions for volcanic surveillance. Advanced UAV, 2 (2), 86-99.

Keywords
Gas Detection
Atmospheric Chemistry
Volcanology
Climate Change
Volcanic Plume
Sniffer4D
Drones

Research Article
Received: 06.10.2022
Revised: 11.11.2022
Accepted: 19.11.2022
Published: 30.11.2022

Abstract

A consistent volcanic monitoring program is crucial to the safety of the population and the efficiency of the nation. Costa Rica´s National Commission for Risk Prevention the CNE helps manage this responsibility. The National Observatory for Volcanoes OVSCORI-UNA and the Atmospheric Chemistry Laboratory LAQAT-UNA of Universidad Nacional Costa Rica through a joint cooperation both have a strategic interest in monitoring and tracking volcanic activity. One aspect of monitoring volcanoes is tracking the active emissions being released from the craters, subaerial and subaqueous fumaroles, and diffuse degassing through soil and cracks. For this study the Sniffer4D gas detection payload was deployed on an UAS and flown directly into the active West Crater of the Turrialba volcano in 2022 for readings of active emissions. The Turrialba volcano is located 40 km or 25 miles East of San José the Capital city of Costa Rica where the majority of the population live. Between 2016-2017 an eruption column emerged 4,000 meters or 13,123 feet above the summit crater of the Turrialba volcano and dispersed ash in the capital resulting in airport closures. Thus, monitoring the Turrialba volcano is of great importance to the country. The UAS system deployed carried the Sniffer4D which tested for Temperature, Humidity and 9 additional parameters - Sulfur Dioxide SO_2 (µg/ m^3), Volatile Organic Compounds VOCs (ppm), Carbon Monoxide CO (mg/m^3), Carbon Dioxide CO_2 (%), Ozone O^3 (µg/ m^3), Nitrogen Dioxide NO_2 (µg/ m^3), O^3+NO_2 and Particulate Matter - PM 1.0, 2.5 & 10**.** The main objective was to characterize the volcanic plume of Turrialba for all of these parameters to establish a baseline that can be built upon in the future through additional measurements to determine changes in outgassing regime of the volcano. This was the first time the Turrialba volcano has been tested for these parameters.

1. Introduction

Volcanic eruptions have long term effects of the atmospheric chemistry of the Earth. Water vapor H_2O, Carbon dioxide CO_2, are the two most abundant gases being released from active volcanoes. These two gases along with Sulfur dioxide SO_2, Hydrogen chloride HCI, Hydrogen fluoride HF, Hydrogen sulfide H_2S are the most common volcanic gases being emitted from active volcano vents. Still there are other trace species such as Hypobromite BrO, One-carbon molecules such as Carbon monoxide CO, Nitrogen dioxide NO_2, Carbon oxysulphide COS, Silicon

tetrafluoride or tetrafluorosilane SiF_4 [1]. H_20 is normally the most abundant gas deriving from a magmatic source and like CO_2 it is relatively abundant in the atmosphere of the Earth. Other volcanic gases such as SO_2, HCI & HF derive from the same source but are not normally present in the atmosphere unless there is an eruption vent releasing these gas species into the nearby proximity.

CO_2 is the second most common gas species being naturally emitted from volcanoes. At the Poás and Turrialba volcanoes in Costa Rica diffuse degassing of CO_2 represents approximately 10% of total emissions abundant in magmatic gas. Diffuse degassing occurs when gas species pass through openings from porous volcanic edifice permeable to rainwater [2]. Researching all aspects of Sulfur dioxide and secondary sulfate aerosols is of strategic importance to the Laboratory of Atmospheric Chemistry because the microphysical dynamics of these particles in active eruption columns is essential to comprehending the radiative properties of these natural volcanic emissions and this is a key to understanding how they affect climatic changes across our planet. Measuring volcanic gases offers insight into subterranean processes happening deep within the Earth's interior [3].

The data collected with the Sniffer4D does contribute to the collective knowledge of the entire scientific community, and the SO_2 tracking data can be cross referenced to the NASA Atmospheric Chemistry and Dynamics Laboratory, Copernicus Atmospheric Monitoring Service European Commission and Global Network of Observation of Volcanic & Atmospheric Change (NOVAC). Active volcanoes releasing emissions have a direct impact on the Earth's atmospheric chemistry, and climatic patterns; therefore, monitoring eruption columns with UAS and gas detection payloads is of extreme importance to climatologists.

Particulates or Particulate Matter can also be measured with the Sniffer4D, data on PM 1.0, 2.5 & 10 can all be gathered**.** Particles also known as atmospheric aerosol particles, atmospheric particulate matter, particulate matter (PM), or suspended particulate matter (SPM) – are microscopic particles of solid or liquid matter suspended in the air. The term aerosol commonly refers to the particulate/air mixture, as opposed to the particulate matter alone. The main objective of launching this payload into the West Crater of Turrialba was completed by Ian Godfrey in 2022.

2. Material and Method

The Sniffer4D was attached to the Mavic 3 and Matrice 600-Pro with an integration kit created with a 3D printer. The Sniffer4D is placed upside down and the 3D printed mounting bracket is placed on top of the bottom of the device. The mounting bracket is then attached with 4 M2.5*6 screws in each corner. The Sniffer4D and attached mounting bracket are then placed onto the Mavic 3 drone and the assembly is permanently connected via 2 additional M2.5*6 screws at the bottom. The Sniffer4D is powered by the same battery as the UAS itself, via a power cable. The power cable aligns to the two outermost power connectors of the Mavic 3 battery. The power cable is secured with three small pieces of double-sided tape and is then attached to the Sniffer4D.The system has a total flight time of around 20 minutes depending on environmental conditions. There are two Sniffer4D Systems one designed for HAZMAT response the S4D and the other to log volcanic emissions S4V which can measure; S4D - NO_2, SO_2, O_2, VOC's, CO_2, CO, PM 1.0, PM 2.5, PM 10, O_3, NO_2+O_3 and S4V - SO_2, CO_2, H_2S, HF, HCI, CO, CxHy/CH_4/LEL, H_2.

Figure 1. Active West Crater of the Turrialba Volcano

The Sniffer4D software program is named Mapper which can showcase the air quality and pollution dispersement as a grid, isoline or 3D plot. The drone was launched from the main lookout point of the Turrialba volcano on the southern edge of the Central Crater. The Sniffer4D can be used to showcase air quality data in real time via a SIM chip and associated data plan placed in the device which is connected to the local cellular network, allowing for real time pollution tracking. Monitoring the SO_2/CO_2 gas ratio is dangerous work, especially during times of increased activity. The device also records temperature and humidity making it an extremely valuable UAS payload for volcanology. Total payload weight was less than 500 grams and can be deployed with gas sampling module which can retrieve volcanic ash and particulate matter which can then be analyzed in the lab.

In 2022 our team reached the summit of the Turrialba volcano on a dry day with clear visibility and no strong or turbulent wind or any other harsh environmental conditions. We were caught in the mud about 4 kilometers or 2.4 miles from the summit crater. After a climb we reached the half-way point where we launched the drone to observe the last stretch of our pathway and make sure there was no significant degassing or explosive activity at the active West Crater. After the first UAS mission we continued our ascent and reached the main lookout point for the Turrialba Volcano National Park. UAS remote sensing approaches have shown exponential potential in the field of volcanology; UAS applications at the Turrialba volcano are a perfect example. The main objective of our UAS survey was to observe the crater interior which we estimated to have crater walls which have slopes of approximately 55^o. The depth of the West Crater was estimated to be 410 feet to 722 feet or 125 meters to 220 meters. The West Crater was estimated to have a width of 620 feet or 189 meters.

The Sniffer4D and Mavic 3 system deployed at Turrialba can help reveal additional valuable data concerning volcanic degassing and emission levels. This measurement system is very useful to the entire scientific community concerning volcanic monitoring and gas emission tracking, volcanic unrest and hazard assessment. Drones using GNSS system fixed waypoints can maneuver around the fumarole location this strategy allows the system to periodically check areas of significant volcanic emission activity and return to the exact same location when necessary. H_2S/SO_2 gas ratios fluctuate depending on temperature, pressure and redox conditions. Significant amounts of SO_2 and H_2S emissions deriving from hydrothermal sources are controlled by this chemical equation: $H_2S + 2H_2O \rightarrow SO_2 + 3H_2$. Increase in SO_2/H_2S represents a potential increase in magmatic influence relative to volcanic emissions [4]. SO_2 emissions represent magmatic intrusion from within the volcanic edifice itself.

Figure 2 & 3. Sniffer4D Mapper Report from the Turrialba Volcano and Associated UAS Image

3. Results

Toxic gas emissions such as Sulfur dioxide or SO_2 which are the direct result of burning fossil fuels contribute to climate change and acid rain in the region. SO_2 is also released from active volcanoes during periods of eruption and UAS are positioned to greatly assist volcanologists measuring these gases from safe distances. UAS capabilities can now greatly assist climate scientists by providing an aerial observation perspective which allows for increased data collection with improved safety. UAS also reduce risks associated with climbing and venturing into regions of increased volcanic activity such as an active crater.

The Sniffer4D detected and provided real time data to team of volcanologists and showcased 9 different gas emissions from one flight into the Turrialba volcano crater. Quantifying total gas flux from an eruption column serves a greater importance than measuring general gas concentration because total gas flux indicative of the level of volcanic outgassing and therefore level of activity [5].

OVSCORI-UNA ranks Turrialba's current level of activity at 3 meaning it is an erupting volcano. There were 2 rumblings on March 27 with no demonstration on the surface. The last Phreatic eruption from Turrialba came on February 28. The OVSCORI-UNA April 1st bulletin explained the daily number of tremors was decreasing. The increase in the amount of SO_2 measured in the atmosphere by satellite means reported the previous week was not confirmed the week of April 1st, 2022 in the weekly report.

The following weekly report showed seismicity remained stable the week of our visit, although there was an increase in the number and duration of short tremors, which are low amplitude. Degassing of Turrialba remained stable, on average weekly CO_2/SO_2 of 22.8 +/- 3.3 and H_2S/SO_2 of 0.25 +/- 0.21. On 7 April 2022, the maximum SO_2 concentration in the ambient air of Coronado (downwind of the Turrialba volcano) was 0.82 ppb and PM10=33.7 $\mu g/m^3$.

The amount of SO_2 measured in the atmosphere by satellite means reported last week remained but without particular trend. Inspection of the bottom of the West Crater with the drone showed some fumaroles at the bottom of the crater mainly in the sector to the east releasing water vapor and sulfur gases. The fumaroles record temperatures of at least 113° F measured remotely with infrared FLIR One Pro thermograph. OVSCORI-UNA April 8st, 2022 weekly report; the week of our visit to the Turrialba crater.

Potential hazards associated with the Turrialba volcano include gases, ash emission, proximal ballistics and acid rain. An active, sleeping or awake volcano can generate eruptions in a way unpredictable, that is, without appreciable precursor signals in real time. In addition, the limited human resources of OVSCORI-UNA do not allow a continuous surveillance of volcanoes. Therefore, the portability and maneuverability of the Sniffer4D is a distinct advantage for these types of institutions tasked with monitoring complex active volcanic systems [6].

Figure 4 & 5. Sniffer4D Flight Path and Image of UAS Mission

Figure 6 & 7. UAS Flight Approaching the Active West Crater

Figure 8 & 9. UAS Flight Arriving at the Active West Crater

During the Sniffer4 UAS test flights at the Turrialba summit a total of 2,424 square meters was covered. The measurement set closest to the active West Crater was taken from the eastern crater rim, although the prevailing winds carry these volcanic emissions to the west. Due to battery capacity and time limitations per flight the eastern rim of the crater was the farthest section the device was sent too. The Sniffer4D recorded a temperature of 22.0877°C or 71.75786°F and Relative Humidity of 19.1234% at the Turrialba summit. Particulate matter log was PM1.0-1.82353, PM2.5-1.88235, PM10-2.05882 for the measurement closest to the crater. Volatile Organic

Compounds were recorded at .187779 ppm. Carbon Monoxide CO was 0.147148 mg/m^3 and Nitrogen Dioxide or NO_2 was 0 µg/m^3. Ozone or O_3 was 1.8456 µg/m^3 and O_3+NO_2 was 1.8456 µg/m^3. The Sniffer4D recorded Sulfur Dioxide or SO_2 at 0 µg/m^3.

The Sniffer4D measurements were taken about 9 meters or 30 feet above the crater floor. In total 17 sections were measured at the Turrialba summit. The Sniffer4D Mapper Software allows for custom visualization. It's possible to adjust the size of the grip on our Mapper to get more specific data. The minimum unit of the grid is 25 square feet, representing that the actual side length of the detection area is 5 meters. The size of the grid indicates the size of the detection area, the smaller the grid is the more specific the data will be and with a higher resolution, to the contrary; the larger the grid is meaning the data will be in a lower resolution and data is calculated by the averaging values from multiple areas. Users can see the general concentration distribution from large grids and then spot the high-concentration area, then they can adjust to small grids and get more specific data in that area.


Figure 10 & 11. Active West Crater of the Turrialba Volcano UAS Sniffer4D Flight Mission


Figure 12 & 13. Active West Crater of the Turrialba Volcano UAS Sniffer4D Flight Mission


Figure 14 & 15. Active West Crater of the Turrialba Volcano UAS Sniffer4D Flight Mission

Comparing the results from the MultiGas and Sniffer4D helped the team learn several lessons for improvement to the methodology. On 7 April 2022 at 1 pm we measured PM10 at 2.05882 µg/m3 with the Sniffer 4D. The same day the maximum PM10 concentrations were 33.7 µg/m^3 at the station in Coronado downwind from the Turrialba volcano. The fluctuations in data show the significance of the prevailing wind direction. SO_2 emissions were recorded at 0 with the Sniffer4D because the prevailing winds carry the gases west. The Sniffer4D was at the eastern crater rim at its closest point. Turrialba is still releasing magmatic gases among them the SO_2. The $S0_2$ module inside the Sniffer4D has a minimum detection limit of 5 ppb for the high-resolution SO_2 and 50 ppb for the wide-range SO_2 modules. The minimum detection limit for particular matter PM2.5 & 10 is 1µg/m^3.

Coronado reports higher concentrations of PM than the measurements carried out by the Sniffer just besides the crater rim because the Sniffer 4D UAS did not measure the entire plume of Turrialba nor did it take a measurement downwind from the active West Crater and therefore the results are very different.

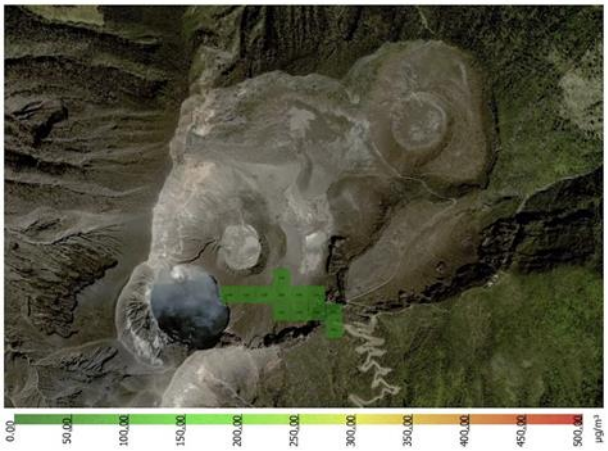

SO_2 Concentration Distribution

Mission Time: 2022/04/07 10:40:07 to 2022/04/07 12:07:37

Sniffer4D DeviceID: 14cd3818 Modual ID: 100

Method: Electrochemical

Number of Samples: 2392

Average Size of the Grid: 49.2375 Meter X 49.2375 Meter (2424.333 Square Meter)

The total detected area: 29092.002 (Square Meter)

Central Coordinates of the Area: -42.3817 W, 10.0189 N

SO_2 Average Concentration: 0.001 µg/m³

SO_2 Maximum Grid Concentration: 0.001 µg/m³ (-83.7607 W, 10.0187 N)

SO_2 Minimum Grid Concentration: 0.000 µg/m³ (-83.7621 W, 10.0187 N)

SO_2 Maximum Point Concentration: 0.611 µg/m³ (-83.7605 W, 10.0182 N) 2022/04/07 10:41:52

SO_2 Minimum Point Concentration: 0.000 µg/m³ (-83.7605 W, 10.0182 N) 2022/04/07 10:40:07

Figure 16 & 17. Sniffer4D Mapper Reports at the Turrialba Volcano for Emissions April 7th, 2022 at 1 pm

The Sniffer Mapper reports minimum, maximum and average SO_2 measurements. Users have the option to load geo tagged photos to contribute to the gas distribution data and final report generated by the software program. Data can be saved to a Micro SD card or data of air quality can be tracked in real time vis an onboard SIM Chip located inside the Sniffer4D V2. The Sniffer Mapper PC Software has a recommended configuration of an Intel i5 core with at least 8 GB of data storage and a 1080p resolution of the screen.

Sniffer Mapper also offers an option to overlay high definition orthophoto overtop of the satellite image map. This option allows for greater direct observation of important degassing regions like fumarolic fields and active volcano craters. This option allows for enhanced observation of the geological changes often associated with volcanic degassing.

Figure 18. AERMOD Plot from April 8th, 2022 the day of investigation with the Sniffer4D the SO2 emission that day was around (151 +- 142) ton/day which was supported by the Sniffer4D data from the crater

The low levels of SO_2 concentration measured by the Sniffer4D at the summit of the Turrialba volcano are consistent with the AERMOD Plot model due to the prevailing wind direction to the west. The Sniffer4D measurement with the UAS was made of the east side of the West Crater of the Turrialba volcano.

Miniaturized gas instrumentation mounted on low-cost drones has enormous potential for safely, rapidly, accurately, and percisely characterizing the gas output of a volcano at all stages of activity. If done carefully, such measurements can be made even when the volcano is erupting. Such an approach allows an excellent snapshot of the current degassing state of an active volcano. Gas ratios and SO_2 fluxes can be measured by drone with data quality comparable to other methods [7].

The complete survey of the Turrialba volcano summit was completed on September 27th, 2022 with the assistance of Universidad Nacional de Costa Rica. We deployed both the Sniffer4D and SnifferV for this complete analysis of volcanic emissions.

1. The first part of the gas emission survey was an aerial measurement conducted by remote pilot in command José Pablo Sibaja Brenes of the Laboratory of Atmospheric Chemistry using the Aki-01 (DJI Matrice 600-Pro). We attached the SnifferV to the Aki-01 in less than 5 minutes and allowed the device to warm up for an additional 5 minutes. The actual flight mission was conducted from 10:43-11:08 am. The flight mission was set for 20 minutes exactly and the Aki-01 was landed successfully with sufficient battery power.

2. The two Sniffer devices were then walked around the active West Crater of the Turrialba Volcano National Park by Dr. Geoffory Avard who passes very close to the fumarolic field where the most obvious degassing occurs. The radius walk around the crater was from 11:10am -12:10pm. It tools one hour to successfully survey the western ridge of the crater which was the most important area due to the trade winds blowing west and dispersing the volcanic gases being released.

3. Central crater walk was from 12:10pm-12:28 and lasted for a total of 18 minutes. The walk through the Central Crater and up to the eastern rim of the West Crater proved to yield some valuable data relative to the state of degassing seen coming from the Turrialba volcano. After the completed analysis we kept the two Sniffer4D V2 units running during our rest period and during the return walk to our starting point at the main lookout point located on the southern crater edge at the summit of the Turrialba volcano. The complete survey was finished at 1:22pm Costa Rica time just before the cloud coverage moved in.

4. Multi-GAS Comparison - The data sets collected at the summit of the Turrialba volcano which were obtained as separate measurement sets can be combined using the Sniffer Mapper software which allowed us to combine these individual measurements to review and evaluate the total ambient air quality for the summit of the Turrialba volcano as a whole.

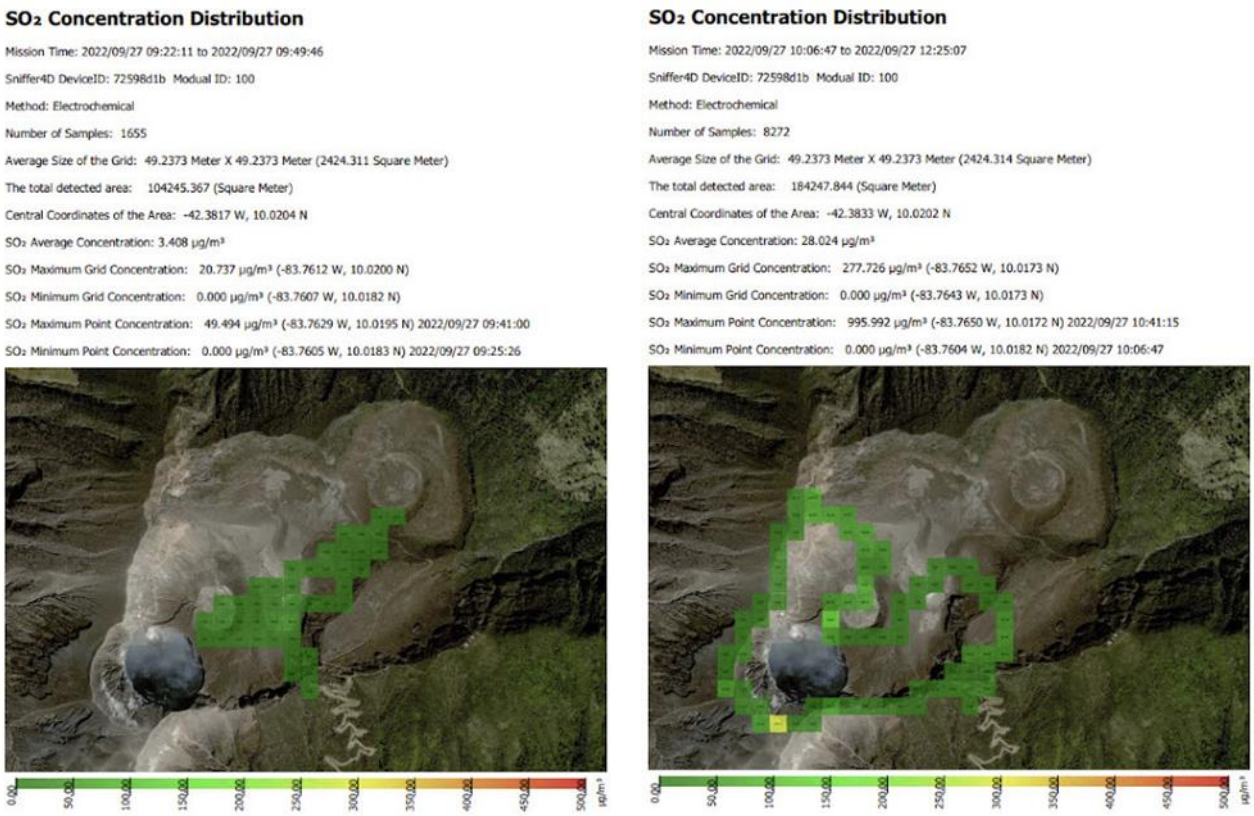

Figure 19 & 20. Reports from Sniffer Mapper software program

SO_2 Concentration Distribution

Mission Time: 2022/09/27 09:22:11 to 2022/09/27 12:25:07

Sniffer4D DeviceID: 72598d1b Modual ID: 100

Method: Electrochemical

Number of Samples: 9927

Average Size of the Grid: 49.2373 Meter X 49.2373 Meter (2424.314 Square Meter)

The total detected area: 247280.000 (Square Meter)

Central Coordinates of the Area: -42.3833 W, 10.0202 N

SO_2 Average Concentration: 25.233 µg/m³

SO_2 Maximum Grid Concentration: 277.726 µg/m³ (-83.7652 W, 10.0173 N)

SO_2 Minimum Grid Concentration: 0.000 µg/m³ (-83.7643 W, 10.0173 N)

SO_2 Maximum Point Concentration: 995.992 µg/m³ (-83.7650 W, 10.0172 N) 2022/09/27 10:41:15

SO_2 Minimum Point Concentration: 0.000 µg/m³ (-83.7605 W, 10.0183 N) 2022/09/27 09:25:26

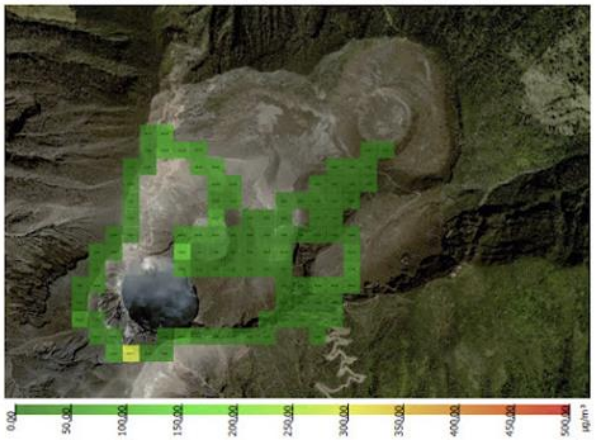

H_2S Concentration Distribution

Mission Time: 2022/09/27 09:22:11 to 2022/09/27 12:25:07

Sniffer4D DeviceID: 72598d1b Modual ID: 100

Method: Electrochemical

Number of Samples: 9927

Average Size of the Grid: 49.2373 Meter X 49.2373 Meter (2424.314 Square Meter)

The total detected area: 247280.000 (Square Meter)

Central Coordinates of the Area: -42.3833 W, 10.0202 N

H_2S Average Concentration: 56.061 µg/m³

H_2S Maximum Grid Concentration: 802.446 µg/m³ (-83.7652 W, 10.0173 N)

H_2S Minimum Grid Concentration: 0.000 µg/m³ (-83.7643 W, 10.0173 N)

H_2S Maximum Point Concentration: 2514.865 µg/m³ (-83.7650 W, 10.0172 N) 2022/09/27 10:41:22

H_2S Minimum Point Concentration: 0.000 µg/m³ (-83.7604 W, 10.0182 N) 2022/09/27 09:24:38

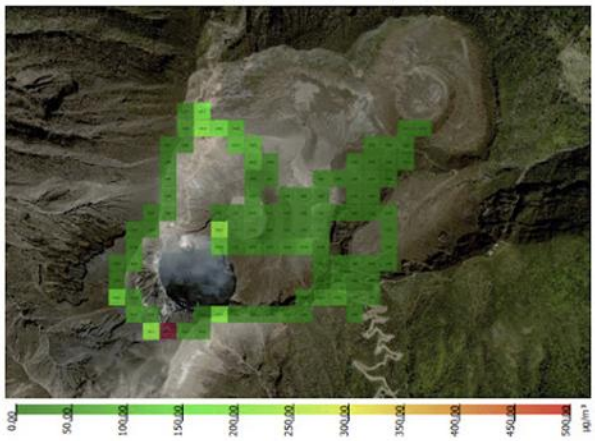

Figure 21 & 22. Reports from Sniffer Mapper software program

	A	B	C	D	E	F	G	H	I	J	K	L	M	N	O	P
1	#Created by: Sniffer4DMapper 2.2.05.25															
2	ProjectName : Turrialba Volcano UNA :															
3	Time Stamp	Abs.Alt m	Longitude	Latitude	Temperat	Humidity	Pressure Pa	SO2 µg/m³	CO mg/m³	CxHy/F	H2S µg/m³	HCL mg/m³	CO2 mg/m³	HF mg/m³	H2 %	Serial No.
4	2022-09-27 09:22:11	0	-83.7604	10.01824	17.2549	42.94118	69340.13281	25.052549	0.464049	0.1914	108.49822	6.842638	1040.30627	13.67286	0	72598d1b
5	2022-09-27 09:22:12	0	-83.7604	10.01824	17.2549	42.94118	69340.13281	24.441511	0.467674	0.1913	110.26242	6.837671	1041.8053	13.66789	0	72598d1b
6	2022-09-27 09:22:13	0	-83.7604	10.01824	17.2549	42.94118	69340.13281	24.441511	0.467674	0.1912	111.14452	6.845122	1037.30823	13.67037	0	72598d1b
7	2022-09-27 09:22:14	0	-83.7604	10.01824	17.2549	42.94118	69340.13281	24.441511	0.471299	0.191	111.14452	6.845122	1038.80725	13.68031	0	72598d1b
8	2022-09-27 09:22:15	0	-83.7604	10.01824	17.2549	42.94118	69340.13281	23.830473	0.471299	0.191	112.02663	6.840155	1041.8053	13.68528	0	72598d1b
9	2022-09-27 09:22:16	0	-83.7604	10.01824	17.2549	42.94118	69340.13281	23.830473	0.467674	0.1909	112.02663	6.845122	1040.30627	13.68776	0	72598d1b
10	2022-09-27 09:22:17	0	-83.7604	10.01824	17.2549	42.94118	69340.13281	23.830473	0.464049	0.1908	112.02663	6.857541	1040.30627	13.68279	0.000008	72598d1b
11	2022-09-27 09:22:18	0	-83.7604	10.01824	17.2549	42.94118	69340.13281	23.830473	0.460423	0.1907	112.90872	6.864992	1038.80725	13.68776	0.000008	72598d1b
12	2022-09-27 09:22:19	0	-83.7604	10.01824	17.2549	42.94118	69340.13281	23.830473	0.464049	0.1907	112.90872	6.872443	1035.80933	13.69521	0.000008	72598d1b
13	2022-09-27 09:22:20	0	-83.7604	10.01824	17.2549	42.94118	69340.13281	23.219435	0.464049	0.1907	113.79082	6.872443	1038.80725	13.70266	0.000015	72598d1b
14	2022-09-27 09:22:21	0	-83.7604	10.01824	17.2549	42.94118	69340.13281	23.219435	0.464049	0.1906	114.67292	6.874926	1035.80933	13.69521	0.000015	72598d1b
15	2022-09-27 09:22:22	0	-83.7604	10.01824	17.2549	42.94118	69340.13281	23.219435	0.467674	0.1905	114.67292	6.874926	1037.30823	13.70266	0.000015	72598d1b
16	2022-09-27 09:22:23	0	-83.7604	10.01824	17.2549	42.94118	69340.13281	22.608398	0.467674	0.1905	115.55502	6.872443	1035.80933	13.7126	0.000015	72598d1b
17	2022-09-27 09:22:24	0	-83.7604	10.01824	17.2549	42.7451	69340.13281	22.608398	0.474925	0.1905	115.55502	6.869959	1035.80933	13.72005	0.000008	72598d1b
18	2022-09-27 09:22:25	0	-83.7604	10.01824	17.2549	42.94118	69340.13281	22.608398	0.474925	0.1904	116.43712	6.867475	1035.80933	13.72998	0.000008	72598d1b
19	2022-09-27 09:22:26	0	-83.7604	10.01824	17.2549	42.7451	69340.13281	22.608398	0.471299	0.1904	117.31921	6.860024	1037.30823	13.73743	0.000008	72598d1b
20	2022-09-27 09:22:27	0	-83.7604	10.01824	17.2549	42.94118	69340.13281	21.99736	0.471299	0.1904	117.31921	6.855057	1037.30823	13.74985	0	72598d1b
21	2022-09-27 09:22:28	0	-83.7604	10.01824	17.2549	42.7451	69340.13281	21.99736	0.471299	0.1904	117.31921	6.855057	1035.80933	13.76476	0	72598d1b
22	2022-09-27 09:22:29	0	-83.7604	10.01824	17.2549	42.7451	69340.13281	21.386322	0.471299	0.1904	117.31921	6.860024	1037.30823	13.77966	0	72598d1b
23	2022-09-27 09:22:30	0	-83.7604	10.01824	17.2549	42.94118	69340.13281	21.386322	0.471299	0.1904	117.31921	6.860024	1035.80933	13.78463	0	72598d1b
24	2022-09-27 09:22:31	0	-83.7604	10.01824	17.2549	42.94118	69340.13281	20.775284	0.471299	0.1903	118.20131	6.857541	1037.30823	13.79953	0	72598d1b
25	2022-09-27 09:22:32	0	-83.7604	10.01824	17.2549	42.94118	69340.13281	20.164248	0.467674	0.1903	119.08342	6.852572	1038.80725	13.80449	0	72598d1b

Figure 23. Reports from Sniffer Mapper software program and CSV Excel Sheet

Figure 24. Sniffer4D Data on SO_2 Showcased on the Sniffer Mapper software program

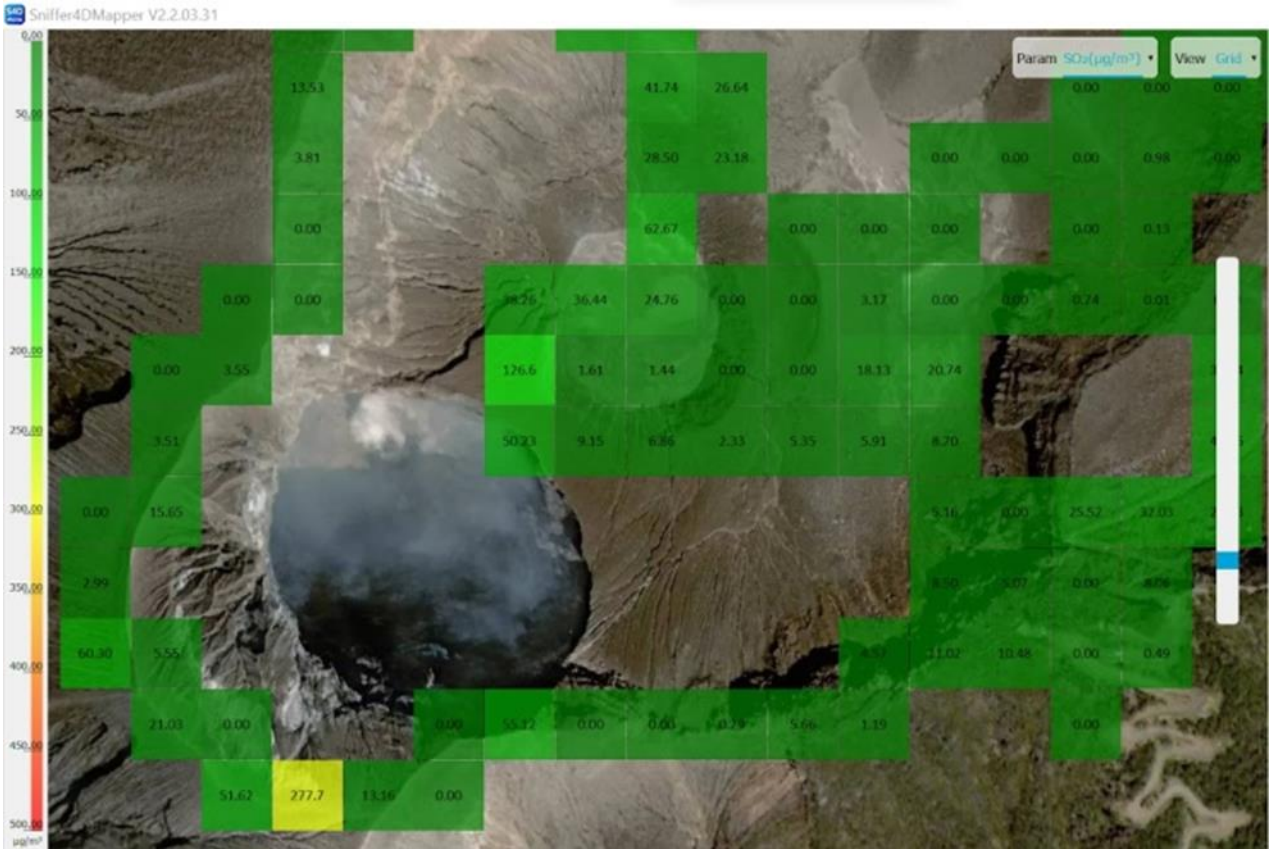

Figure 25. Sniffer4D Data on SO_2 Showcased on the Sniffer Mapper software program

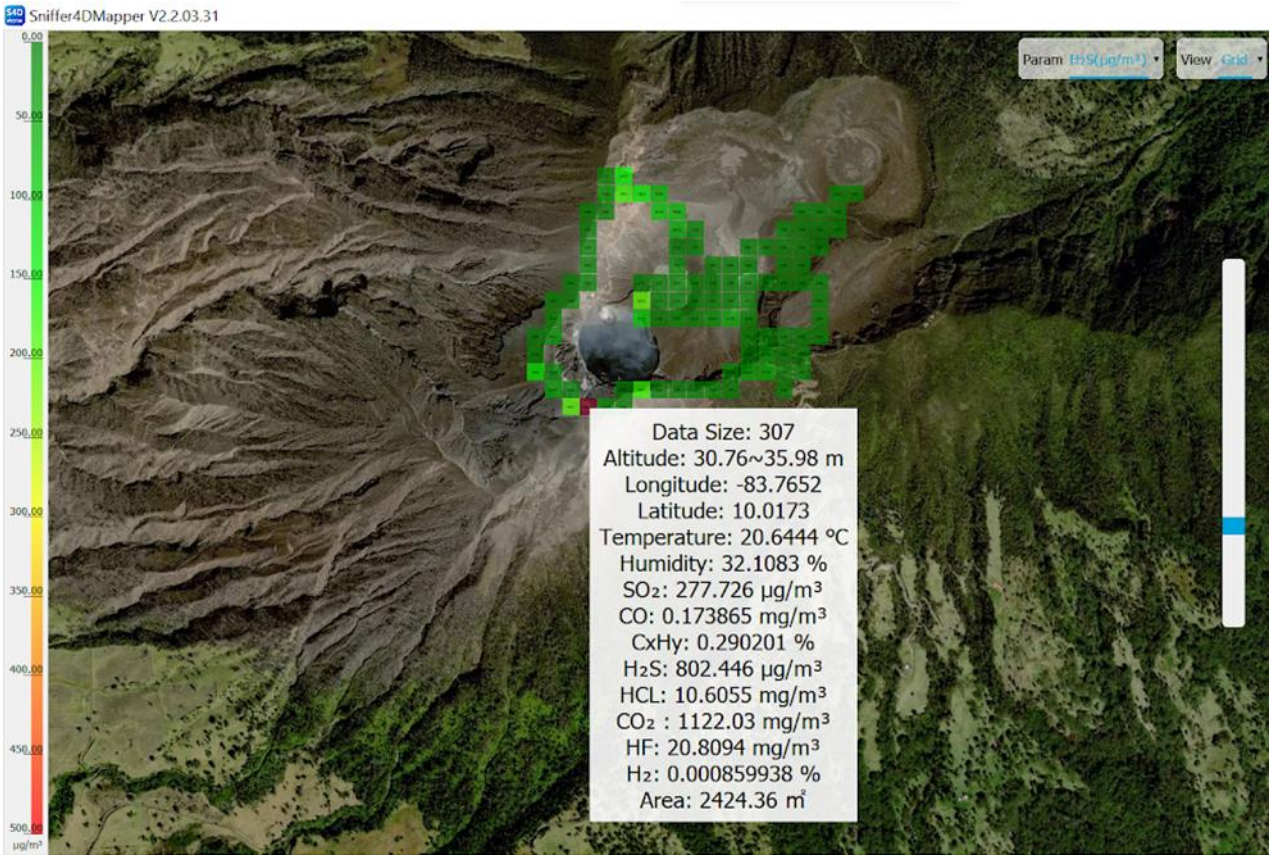

Figure 26. Sniffer Mapper High Level Gas Detection Reading Example

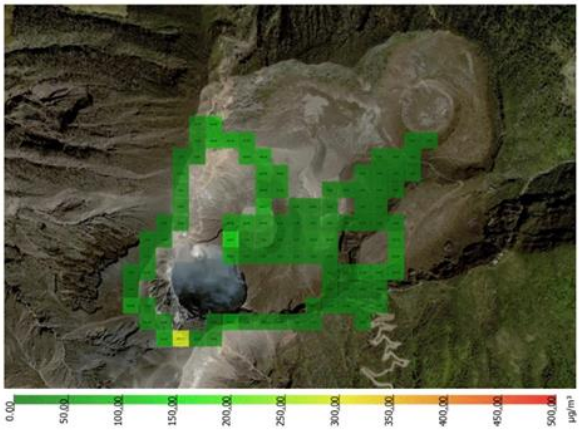

SO_2 Concentration Distribution

Mission Time: 2022/09/27 09:22:11 to 2022/09/27 12:25:07

Sniffer4D DeviceID: 72598d1b Modual ID: 100

Method: Electrochemical

Number of Samples: 9927

Average Size of the Grid: 49.2373 Meter X 49.2373 Meter (2424.314 Square Meter)

The total detected area: 247280.000 (Square Meter)

Central Coordinates of the Area: -42.3833 W, 10.0202 N

SO_2 Average Concentration: 25.036 μg/m³

SO_2 Maximum Grid Concentration: 277.726 μg/m³ (-83.7652 W, 10.0173 N)

SO_2 Minimum Grid Concentration: 0.000 μg/m³ (-83.7643 W, 10.0173 N)

SO_2 Maximum Point Concentration: 995.992 μg/m³ (-83.7650 W, 10.0172 N) 2022/09/27 10:41:15

SO_2 Minimum Point Concentration: 0.000 μg/m³ (-83.7605 W, 10.0183 N) 2022/09/27 09:25:26

Figure 27 & 28. Sniffer4D V2 SO_2 Reading and Sniffer Mapper Software System

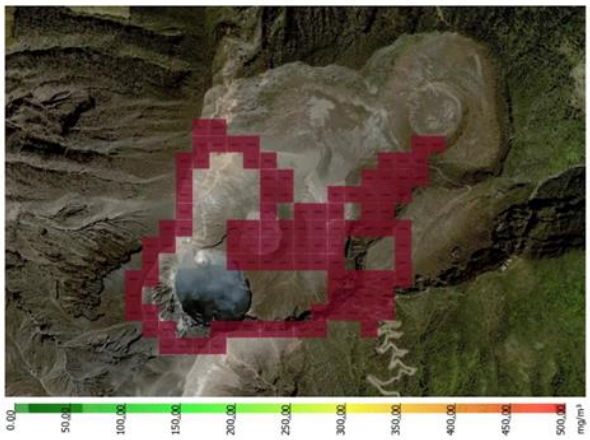

CO_2 Concentration Distribution

Mission Time: 2022/09/27 09:22:11 to 2022/09/27 12:25:07

Sniffer4D DeviceID: 72598d1b Modual ID: 100

Method: Electrochemical

Number of Samples: 9927

Average Size of the Grid: 49.2373 Meter X 49.2373 Meter (2424.314 Square Meter)

The total detected area: 247280.000 (Square Meter)

Central Coordinates of the Area: -42.3833 W, 10.0202 N

CO_2 Average Concentration: 1071.210 mg/m³

CO_2 Maximum Grid Concentration: 1228.731 mg/m³ (-83.7634 W, 10.0204 N)

CO_2 Minimum Grid Concentration: 1028.864 mg/m³ (-83.7612 W, 10.0213 N)

CO_2 Maximum Point Concentration: 1572.451 mg/m³ (-83.7650 W, 10.0172 N) 2022/09/27 10:41:06

CO_2 Minimum Point Concentration: 1022.318 mg/m³ (-83.7625 W, 10.0213 N) 2022/09/27 11:22:59

Figure 29 & 30. Sniffer4D V2 CO_2 Reading and Sniffer Mapper Software System

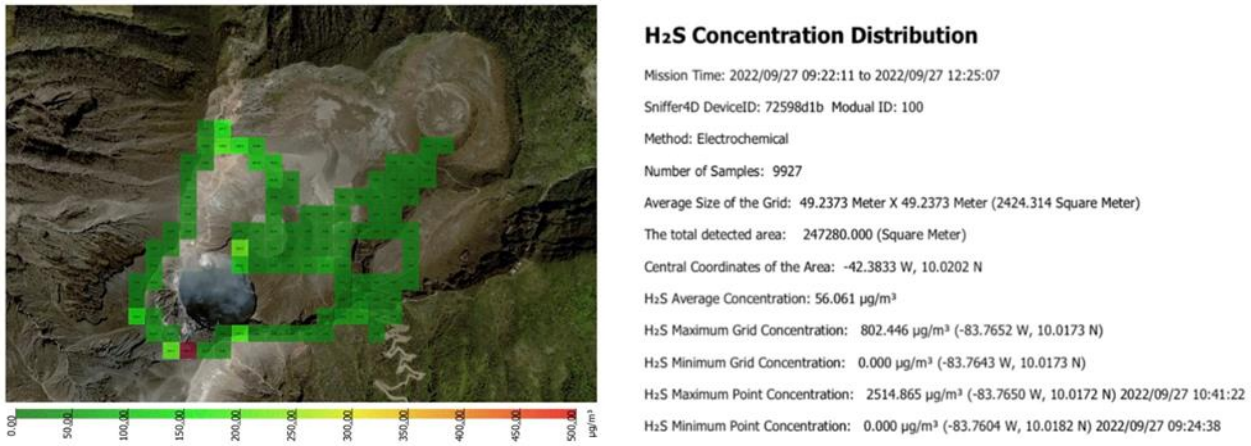

Figure 31 & 32. Sniffer4D V2 H_2S Reading and Sniffer Mapper Software System

4. Discussion

UAS are allowing scientists to deliver new scientific equipment into the most extreme environments and take physical samples of water along with atmospheric parameters yielding a vast amount of valuable information not previously accessible before the implementation of UAS. Recent development of new remote sensing technologies has not only made it easier to obtain information, but has also made it possible to extract data across larger and more dangerous areas. In this sense, we can also cite in addition to UAVs, the famous LiDAR (Light Detection and Ranging), which is an emerging technology aimed at collecting accurate data in a shorter

period of time and using the distance between the target and the laser. Pershin et al. [8] have done the monitoring of the Elbrus volcano using LiDAR based diode laser. Their results highlight the effective role of laser to detect and monitor such type of volcanoes.

PM and SO_2 test flight with the Mavic 3 was successful. Piloting remote aircraft in high altitude volcanic environments is one of the most complex and risky situations for a drone pilot. Is the data more valuable than the drone? Is a frequent question remote pilots often ask themselves before the flight and at the point in the flight where the drone begins collecting great data, prized photos and excellent video, but riskier conditions start settling in. For example, of a complex flight for a remote pilot operating in a volcanic environment is when it's clear where the drone around 600 meters away from the home point and it starts raining at the remote pilot's location. These situations must be planned for to the best if the remote pilot in command capabilities. Unaccounted for situations will still arise, but with proper training and knowledge of these environments obtaining the data points from the planned flights is certainly possible. When planning to operate drones in volcanic environments it's essential to check the weather forecasts for the days you're planning the mission and to consistently monitor any potential changes on Windy.

Figure 33 & 34. UAS Perspective observing the interior of the Active West Crater

Climatic stability in volcanic regions can change in less than one minute. And with that comes relative humidity fluctuations, 80% change in visibility conditions, wind speed change, wind direction change, enhancing wind gusts. Therefore, extreme presentation is necessary for the remote pilot to obtain as much geological and atmospheric knowledge of the region before flights. In Costa Rica while studying the Turrialba volcano at 3,340 meters in altitude the poor visibility and cloud coverage changes were frequently avoided with the assistance of a visual observer and the decision to increase or decrease altitude to avoid the passing clouds. Obviously, these decisions are made by the remote pilot in command who must also consider the altitude of the flight and the terrain formations directly below the drone. Flying UAS directly above active craters will always add risk of eruption.

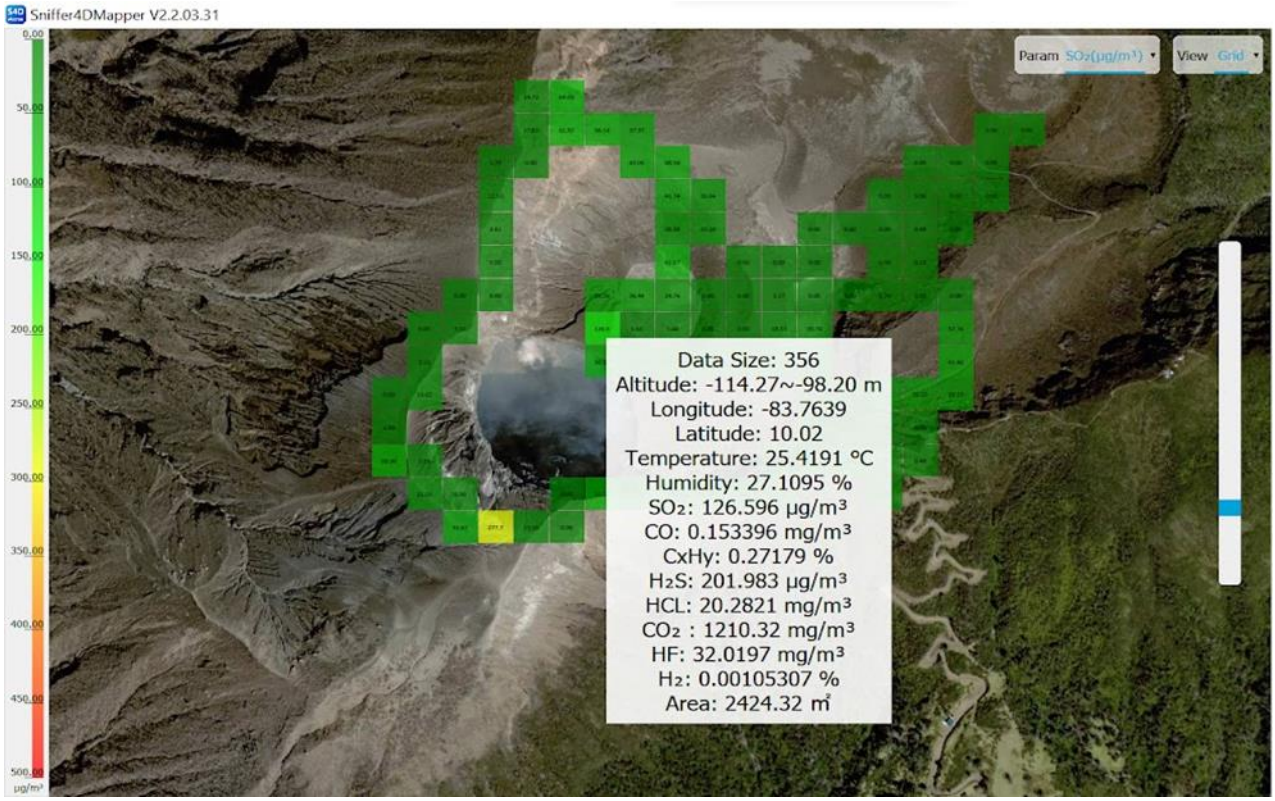

Figure 35. Sniffer Mapper Volcanic Emission Reading of Active West Crater rim of the Turrialba Volcano

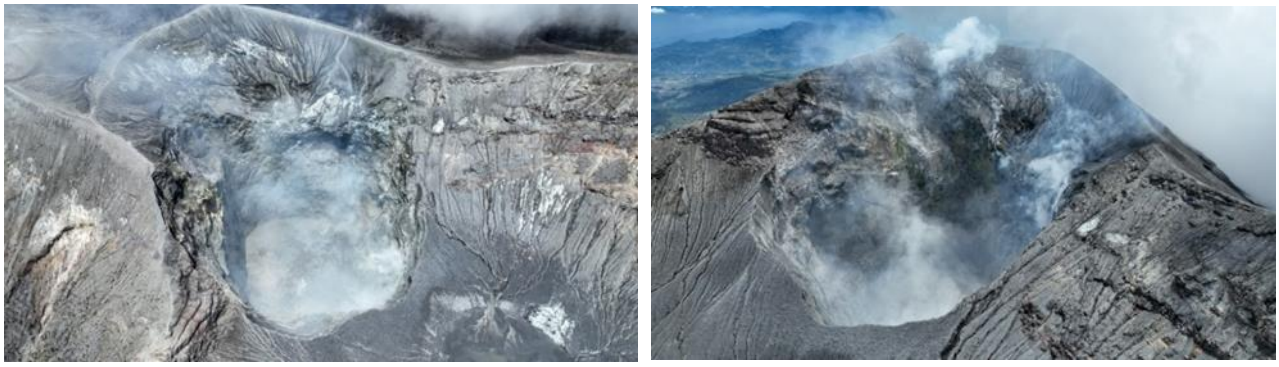

Figure 36 & 37. Active West Crater of the Turrialba Volcano

Figure 38 & 39. Active West Crater of the Turrialba Volcano

5. Conclusion

The monitoring of volcanic gas geochemistry is a vital aspect to understanding volcanic processes. Continuous gas tracking during volcanic eruptions will allow for valuable information to be delivered to scientists which offer insights to how the interior volatiles behaved through the volcanic process from the low activity period through an eruption. The research publication titled *"A golden era for volcanic gas geochemistry"* explains that; "Volatiles

can diffuse through magma bodies, travel latterly along faults, exsolve and re-dissolve in magma or aqueous fluids, or be stored in underground reservoirs from which they can be explosively erupted into the atmosphere or leaked slowly to the surface over millennia." [9].

"The primary components of all high temperature volcanic gases are water vapor (H_2O, typically 75-98%), carbon dioxide (CO_2, 0.3-13%), sulfur dioxide (SO_2, 0.3-3%), and hydrogen sulfide (H_2S, 0.02-2%). Changes in gas composition and emission rate are likely one of the first signs of unrest at volcanoes." By expanding our gas detection capabilities and broadening our UAS application to include volcanic emission tracking, we can begin monitoring more emissions from a larger number of volcanoes and through increased frequency and reliability along with using previously confirmed early warning detection systems and data analysis significant improvements can be made to our strategy and ability to predict volcanic eruptions. Carbon dioxide CO_2 can be from both magmatic sources and hydrothermal as well; this gas can travel along fault lines; it can be periodically released from cracks and fractures in the volcanic edifice and it can also diffuse through soils surrounding the active crater. CO_2 can also be released from soils that are distant from the active crater and fumarolic field making gas measurements important for surveying and tracking emissions in other volcanic areas further away from the areas of visible activity [9].

UAS bridge a significant knowledge gap in volcanic surveillance as they can access areas inaccessible to researchers and can document and collect data in these areas. Since drones can also carry payloads like the Sniffer4D gas detection equipment the inaccessible gas plumes can now be measured and monitored. Several departments and research institutions have dedicated time and resource into tracking volcanic emissions on a global scale and their findings and forecasts can be found in *Network of Observation of Volcanic and Atmospheric Chance (NOVAC) [10], Deep Earth Carbon Degassing (DECADE) [11], The EarthChem/ DECADE database [12], The Mapping Gas Emission Project [13], The NOVAC data portal [14].*

"Aquifers can be primed for eruption by sealing via hydrothermal alterations and mineralization, including buildup of pore fracture filling sulfates, clays, sulfur minerals and silica. However, sealing can be localized or affect extensive areas in these diverse geological environments." [15]. These events can occur suddenly or progressively and are therefore strategically important to monitor for volcanic institutions.

"If lakes occupy active craters they can act as traps for high temperature gases, allowing the formation of molten element sulfur (>114°C) within the aquifer. To data no phreatic or hydrothermal eruption has been successfully forecasted. This presents a significant challenge to volcano observatories and monitoring systems. Continuous gas monitoring provides significant insight into eruption "priming" processes at various time scales. Turrialba with peaks in CO_2/SO_2 prior to eruptive phases in 2014 and 2015 signal magma injection that disrupted the overlying hydrothermal system, whereas the disappearance of H_2S in emissions marked the transition from phreatic to phreatomagmatic activity." [15].

Ambient air monitoring and HAZMAT response have become some of the most prominent applications for miniaturized hardware payloads designed for UAS. Data of the volcanic plume and its effects of atmospheric chemistry are easily collected by the Sniffer4D and analyzed by the software program Sniffer4D Mapper which provides a quick, sustainable, safe and reliable way to quantify these emissions and develop a national baseline for volcanic activity in Costa Rica.

The Sniffer 4D could give promising results if it is flown all around the crater in circles or doing a transect crossing the crater from upwind to downwind. Another advantage of deploying this system is the ability to see vertical profiles of volcanic emissions downwind from the eruption site. This investigation outlines UAS volcanic applications designed to detect and quantify different gases of volcanic origin in order to assist volcanologists with their eruption forecasts.

Acknowledgement

Ian Godfrey is a passionate explorer of the natural world, a writer, a Part 107 Remote Pilot and Thesis Advisor to the Laboratory of Atmospheric Chemistry Universidad Nacional Costa Rica. He has flown UAS into several high altitude active volcanic craters and a variety of industrial sites.

Funding

This research received no external funding.

Author contributions

Ian Godfrey: Conceptualization, Methodology, Software **José Pablo Sibaja Brenes:** Data curation, Writing-Original draft preparation, Software, Validation. **Maria Martínez Cruz:** Visualization, Investigation, **Khadija Meghraoui:** Writing-Reviewing and Editing.

Conflicts of interest

The authors declare no conflicts of interest.

References

1. Platt, U., Bobrowski, N., & Butz, A. (2018). Ground-based remote sensing and imaging of volcanic gases and quantitative determination of multi-species emission fluxes. Geosciences, 8(2), 44.
2. Epiard, M., Avard, G., De Moor, J. M., Martinez Cruz, M., Barrantes Castillo, G., & Bakkar, H. (2017). Relationship between diffuse CO2 degassing and volcanic activity. Case study of the Poás, Irazú, and Turrialba Volcanoes, Costa Rica. Frontiers in Earth Science, 5, 71.
3. Xi, X., Johnson, M. S., Jeong, S., Fladeland, M., Pieri, D., Diaz, J. A., & Bland, G. L. (2016). Constraining the sulfur dioxide degassing flux from Turrialba volcano, Costa Rica using unmanned aerial system measurements. Journal of Volcanology and Geothermal Research, 325, 110-118.
4. Mori, T., Hashimoto, T., Terada, A., Yoshimoto, M., Kazahaya, R., Shinohara, H., & Tanaka, R. (2016). Volcanic plume measurements using a UAV for the 2014 Mt. Ontake eruption. Earth, Planets and Space, 68(1), 1-18.
5. Harvey, M. C., Rowland, J. V., & Luketina, K. M. (2016). Drone with thermal infrared camera provides high resolution georeferenced imagery of the Waikite geothermal area, New Zealand. Journal of Volcanology and Geothermal Research, 325, 61-69.
6. http://www.ovsicori.una.ac.cr/index.php/vulcanologia/informes-y-boletines/boletin-semanal-vigilancia-volcanica/category/70-boletines-semanales-vulcanologia-2022?start=10
7. Stix, J., de Moor, J. M., Rüdiger, J., Alan, A., Corrales, E., D'Arcy, F., ... & Liotta, M. (2018). Using drones and miniaturized instrumentation to study degassing at Turrialba and Masaya volcanoes, Central America. Journal of Geophysical Research: Solid Earth, 123(8), 6501-6520.
8. Pershin, S. M., Sobisevich, A. L., Grishin, M. Y., Gravirov, V. V., Zavozin, V. A., Kuzminov, V. V., ... & Fedorov, A. N. (2020). Volcanic activity monitoring by unique LIDAR based on a diode laser. Laser Physics Letters, 17(11), 115607.
9. Kern, C., Aiuppa, A., & de Moor, J. M. (2022). A golden era for volcanic gas geochemistry?. Bulletin of Volcanology, 84(5), 1-11.
10. https://novac-community.org
11. https://deepcarbon cycle.org/home-decade
12. https://decade.earthchem.org/
13. https://www.magadb.net
14. https://novac.chalmers.se/
15. Montanaro, C., Mick, E., Salas-Navarro, J., Caudron, C., Cronin, S. J., de Moor, J. M., ... & Strehlow, K. (2022). Phreatic and Hydrothermal Eruptions: From Overlooked to Looking Over. Bulletin of Volcanology, 84(6), 1-16.